Preparation and Evaluation of Sol-Gel Made Nickel Catalysts for Carbon Dioxide Reforming of Methane

A Thesis Submitted to the College of Graduate Study and Research

for Partial Fulfillment of the Requirements

for the Degree of Master of Science

in the Department of Chemical Engineering

University of Saskatchewan

Saskatoon

By

Haijun Sun

PERMISSION TO USE

In presenting this thesis in partial fulfillment of the requirements for a postgraduate degree from the University of Saskatchewan, I agree that the libraries of this University may make it freely available for inspection. I further agree that permission for copying of this thesis in any manner, in whole or in part, for scholarly purposes may be granted by the professor or professors who supervised my thesis work or, in their absence, by the Head of the Department or the Dean of the College in which my thesis work was done. It is understood that any copying or publication or use of this thesis or parts thereof for financial gain shall not be allowed without my written permission. It is also understood that due recognition shall be given to me and to the University of Saskatchewan in any scholarly use which may be made of any material in my thesis.

Requests for permission to copy or to make other use of material in this thesis in whole or part should be addressed to:

Head of the Department of Chemical Engineering_____

University of Saskatchewan

Saskatoon, Saskatchewan (S7N 5A9)

ABSTRACT

Sol-gel (solution-gelation) method was used to prepare Ni-Ti and Ni-Ti-Al catalysts for reforming of methane with carbon dioxide. This method, after optimizing the parameters such as hydrolysis and acid/alkoxide ratio, is able to make a Ni-Ti catalyst with a surface area as high as 426m^2/g when calcined at 473K; but calcination at higher temperature lead to dramatic decrease in surface area. XRD, XPS, TEM and SEM were used to understand this change.

Using a packed bed reactor, the catalysts were evaluated with the reforming reaction. It was found that the activity of the Ni-Ti catalyst increases with the Ni loading in the range of 1-10wt%. The reduction temperature has strong effect on activity of the reduced catalyst. Up to 973K, the activity increases with the reduction temperature; but after 973K, the activity decreases and become 0 when the temperature is over 1023K. The Ni-Ti catalyst also deactivated as 15% after 4h of time on stream. The XRD analysis shows that Ti_3O_5 formed in the catalyst after higher-temperature reduction as well as after the reaction for a period of time. The formation of Ti_3O_5 may render the catalyst to loss its activity. However, further study is expected to understand the mechanism. TG/DTA analysis shows that both Ni-Ti and Ni-Ti-Al catalysts had carbon deposition; but the latter maintained higher activity in a longer period of time.

ACKNOWLEDGEMENTS

I wish to give my sincere gratitude to my supervisor Dr. Hui Wang. I thank him for his valuable advices and patient tutoring on such a wonderful project. His enthusiasm and support kept me on track and his standard of excellence has given me the momentum to pursue to higher level.

My sincere thanks go to other professors in my advisory committee, Dr. Ajay K. Dalai and Dr. Todd Pugsley. Their encouragement, continuous instructions and ideas were invaluable for the completion of this project.

I would also like to thank the colleagues and fellow students I had the pleasure to work with during this project: Christian Botchwey, Abena Owusu-Boakye, Ramin Azargohar, Dr. Deena Ferdous, Dr. Rajesh Gopinath, Nikhil Das, Dragan Cekic, Richard Blondin, Ted Wallentiny. I would specially thank Jianguo Zhang for his friendship and support both in and out of the workplace.

I also thank the Natural Sciences and Engineering Research Council (NSERC) for its financial support to this project.

DEDICATION

TO MY WIFE JUAN AND MY DAUGHTER CATHERINE-LE

TABLE of CONTENT

LIST of TABLES

LIST of FIGURES

ABBREVIATIONS

CCD: Central Composite Design

DRM: Dry Reforming of Methane

GHGs: Greenhouse gases

LV: Linear Velocity, m/s

MFC: Mass Flow Controller

RSM: Methodology of Response Surface

RWGS: Reverse Water-Gas Shift

SA: Surface Area (m^2/g)

SEM: Scanning Electron Microscopy

SMSI: Strong Metal-Support Interaction

SV: Space Velocity, SCCM/g-cat/h

TEM: Transmission Electron Microscopy

TGA: Thermogravimetric Analysis

TG/DTA: Thermal Gravity/Differential Thermogravimetric Analysis

TOF: Turn Over Frequency

TPO: Temperature Programmed Oxidation

TPH: Temperature Programmed Hydrogenation

WGS: Water Gas Shift

XRD: X-ray Diffraction

XPS: X-ray Photoelectron Spectroscopy

NOMENCLATURE

A_{BET}	BET surface area (m^2/g)
AC	Acid/alkoxide ratio
at%	Atomic percentage
H	Hydrolysis ratio, the ratio of water to alkoxide
ΔH	Reaction enthalpy (kJ/mol)
m	Coordination number
M	Transition metals
R	Alkyl or aryl group
$R_{average}$	Average pore diameter (Å)
wt%	Weight percentage
X	Alkyl group or hydrogen

CHAPTER 1

INTRODUCTION

1.1 Background of the Project

Carbon dioxide is released into the atmosphere when fossil fuels such as oil, natural gas, and coal are burned. As a result of the tremendous world-wide consumption of such fossil fuels, the concentration of CO_2 in the atmosphere has increased over the past century, now rising at a rate of about 1ppm per year, estimated to be around 2×10^{15}g of carbon per annum [1]. The increase in the concentration of greenhouse gases (GHGs), particularly CO_2, in the atmosphere is believed to be responsible for the major changes in global climate. A correlation of mean global temperature rise with atmospheric CH_4 and CO_2 concentration, drastic changes in the annual temperature cycle of the Northern Hemisphere, and increasing volatility of global weather patterns have been reported [1]. In order to reduce the emitting rate of CO_2 into the atmosphere, most industrialized countries were required to reduce their GHGs emissions by the Kyoto Protocol, in which Canada is expected to reduce its GHGs emissions to 6% below the 1990 levels in the coming decade. Tremendous adverse impacts on national and provincial economy would be resulted if the emissions are forced to be reduced without economically justifiable technologies which are able to transfer CO_2 into value-added materials or with low

operation cost. Consequently, there has been increased interest in a better understanding of CO_2 removal, disposal, utilization and CO_2 permanent sequestration.

A lot of new initiatives for CO_2 sequestration have been raised, examples including CO_2 sequestration in geological formations including oil and gas reservoirs, unmineable coal seams, and deep saline reservoirs; direct injection of CO_2 into deep ocean and stimulation of phytoplankton growth; terrestrial sequestration of CO_2 with natural resources like vegetation and soils [2]; and mineral carbonation [3,4] to permanently sequester CO_2 by injecting it into deep underground well and detained by reacting with stones to form carbonate. However, all these initiatives are far from mature with tremendous technical and scientific difficulties to overcome. Possible spill of CO_2 in the future is another concern of these technologies. Thus it is more attractive to sequester CO_2 by converting it into value added products via chemical reactions.

Reforming of CH_4 with CO_2, also known as dry reforming of methane (DRM), which was originally initiated by J. Lang in 1888 and thoroughly explored by Fischer and Tropsch in 1928 [5], has become the preeminent reaction to convert these two reactants. DRM, combining two prominent greenhouse gases, CO_2 and CH_4, is regarded as a potential route to sequester CO_2 by converting them into value added products, synthesis gas ($CO+H_2$), from which many commodity chemicals and products can be produced. As the advanced and cost effective CO_2 separation technologies are developed, pure CO_2 feed stream can be obtained for the DRM. In addition, DRM unit can be built along with the power plant, which discharges one third of the total CO_2 emission, to save the cost for storage and transportation.

DRM also demonstrates the other advantages. Due to its strong endothermic character, it is regarded as a potential route to store and transmit energy. The effluent syngas, with a ratio of H_2/CO less than unit, is a preferred feedstock for the Fischer-Tropsch reaction to produce higher hydrocarbons and oxygenated derivatives [6]. DRM also supplies an alternative to produce hydrogen which is widely used in different industries, such as bitumen upgrading, refining, and now in proton exchange membrane fuel cells.

Although DRM has shown great economic and environmental advantages, realization of this process is full of difficulties. DRM is a strong endothermic reaction. It requires a very high temperature (>1123K) to obtain an acceptable conversion. Without the presence of a catalyst, the reaction rate is too slow to be economically justifiable, and, in addition, a large amount of char may form due to the crack of CH_4 and disproportionation of CO. These difficulties necessitate the presence of a catalyst which can accelerate the reaction at an industrially feasible temperature (<1023K) and kinetically inhibit the char formation.

During the past two decades, numerous studies have been conducted attempting to understand the mechanism of the DRM reaction on different catalysts and to develop industrially usable catalysts [1,7,8]. Most group VIII metals are catalytically active for this reaction. The characters of active metals, supports and methods of preparations have significant effect on the performance of catalysts [1]. Though noble metals, such as Pt, and Rh, were reported more resistant to char deposition [1], nickel is regarded as the most prominent active component due to its wider availability and lower cost. As one of the most used catalyst supports, titania has been proven the ability to decrease carbon

deposit [1]. It was also reported that the strong metal-support interaction could promote the dispersion of active metal and mitigate the carbon formation, and the sol-gel catalyst preparation method can improve the interaction between metals. Although Ni-Ti catalyst made by sol-gel has been investigated for other reactions [9], its performance for DRM at high temperature (above 900K) remains unknown.

1.2 Scope and Outline of the Work

The hypothesis for this project is that Ni-Ti catalyst made by sol-gel has stronger interaction between components and the interaction would help to inhibit carbon formation, thus prolonging the life of the catalyst. The work of this project comprises of two parts: preparation of Ni-Ti catalysts using sol-gel method and evaluation of the sol-gel made Ni-Ti catalysts with DRM. In the catalyst preparation part, the factors which influence the surface area and pore structures are to be optimized. The results will provide reference for future preparation of sol-gel Ni-Ti catalysts as well as nano materials. Instrumental characterizations which could help understand the correlations between influential factors will be conducted. In the catalyst evaluation part, several factors which influence the performance of catalysts will be evaluated. The post reaction characterizations will be conducted to explain the experimental results. Based on the experimental results, in order to improve the performance of catalyst, some modifications to the catalyst system will be conducted.

This thesis consists of 5 chapters, including the literature review, experimental procedures, results and discussion, conclusions and recommendations. Following this chapter, chapter 2 discusses the fundamentals of DRM including the reactions involved

and their chemistry and thermodynamics, the development in catalysts for DRM, and the sol-gel method of catalyst preparation, reasoning out the objectives of this research. Chapter 3 introduces the experimental procedures and instrumental analysis used in this research, including equipment, chemicals and other materials. Chapter 4 presents the experimental results, gives the respective discussion and leads to conclusions. Chapter 5 lists the research conclusions drawn from Chapter 4, and also includes recommendations for future research.

CHAPTER 2

LITERATURE REVIEW

2.1 Reaction Chemistry

The reaction equilibrium for the production of synthesis gas from CH_4 and CO_2,

$$CH_4 + CO_2 \rightleftharpoons 2H_2 + 2CO \qquad (\Delta H^0 = 247.3 \text{ kJ/mol } CH_4) \qquad (1)$$

is influenced by the simultaneous occurrence of the reverse water-gas shift (RWGS) reaction

$$CO_2 + H_2 \rightleftharpoons CO + H_2O \qquad (\Delta H^0 = 41.17 \text{ kJ/mol}) \qquad (2)$$

which results in H_2/CO ratio less than unity. The overall equilibrium conversion of CH_4 and CO_2 and the H_2/CO and H_2O/CO ratios of these two reactions for a feed stream at a total pressure of 1 atm (CH_4/ CO_2/He = 1/1/1.8) are shown in Figure 2.1 [1]. The conversion of CO_2 is always greater than that of CH_4, due to the RWGS equilibrium. In practice, this is advantageous when producing gas streams with a H_2/CO ratio of 1 or lower are necessary. For example, to produce alkanes directly from synthesis gas, the following reaction stoichiometry is observed:

$$2nCO + (n + 1)H_2 \rightleftharpoons C_n H_{(2n+2)} + nCO_2 \qquad (3)$$

and the required H_2/CO feed ratio is (n + 1)/2n, which is less than or equal to unity.

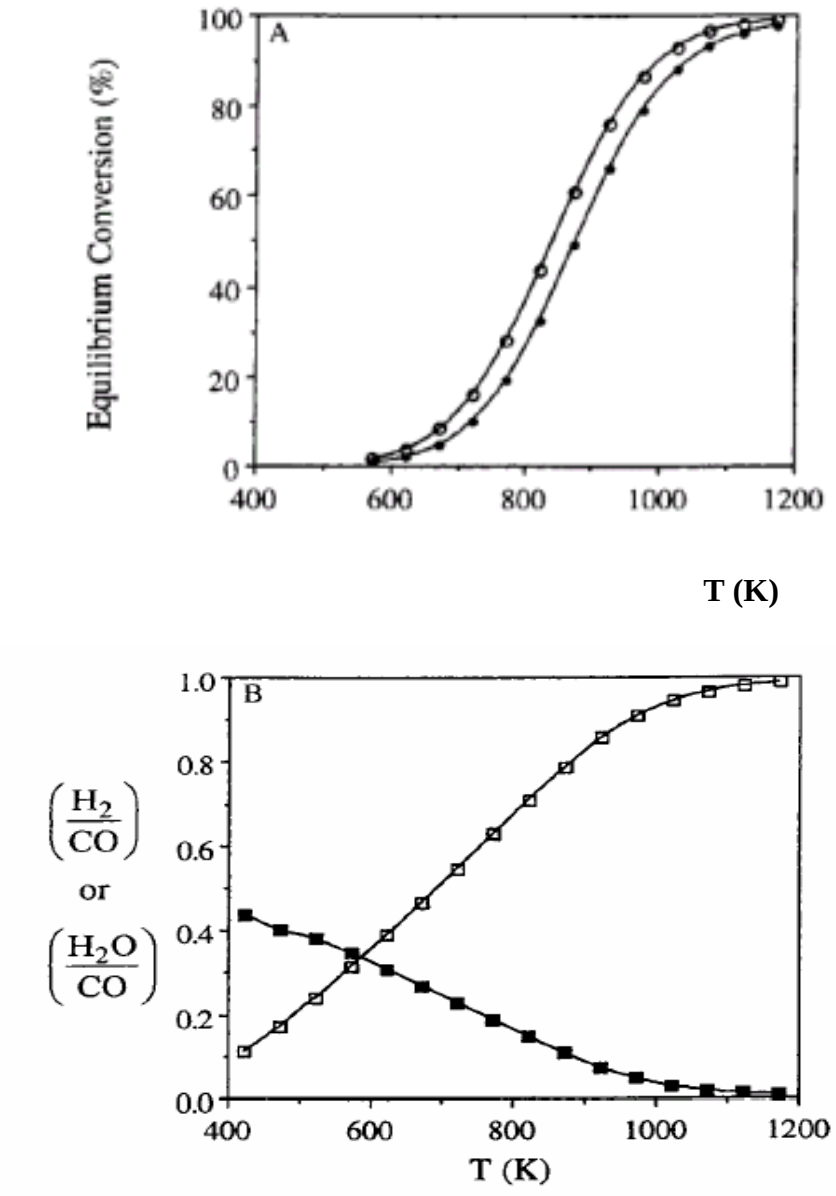

Figure 2.1. (A) Equilibrium conversions of CO_2 (○) and CH_4 (●), (B) product ratios of H_2/CO (□) and H_2O/CO (■) for simultaneous CO_2-CH_4 reforming and RWGS reactions as a function of temperature. Reaction conditions: P_{tot} = 1atm; $CH_4/CO_2/He$ = 1/1/1.8 [1].

As shown in Figure 2.1, it is thermodynamically preferable for DRM when the reaction temperature is more than 1000K. However, due to safety and economic concerns, it is preferred to operate the reaction at low temperature from the industrial standpoint. In addition to the DRM and RWGS reactions, there are two other side reactions which occur simultaneously. The CH_4 decomposition

$$CH_4 \rightleftharpoons C(s) + 2H_2 \qquad (\Delta H^0 = 74.85 \text{ KJ/mol}) \tag{4}$$

and CO disproportionation

$$2CO \rightleftharpoons CO_2 + C\ (s) \qquad (\Delta H^0 = -173.46 \text{ KJ/mol}) \tag{5}$$

These two reactions are directly responsible for the carbon deposition on the catalyst. If the reaction temperature is lowered to a range from 800~900K, it is more preferential to carbon depositions than to DRM. Therefore, a catalyst which can kinetically inhibit the carbon formation and simultaneously improve the DRM reaction rate appears very necessary.

2.2 Catalyst Development

Most group VIII metals are active for DRM. Although noble metal containing catalysts, such as Pt [10] and Rh [7], have shown better properties in stability and carbon deposition resistance than Ni catalysts, Ni was chosen as the active metal in this project due to its wider availability. Table 2.1 shows the Ni-containing catalysts have been investigated for DRM. Most Ni catalysts have shown competitive activity [1], and some of them are relatively stable when certain type of supports are employed [11,12].

Table 2.1. Ni-containing catalysts investigated for DRM

Support	Reference	Support	Reference
Al_2O_3	13,14	MgO/CaO	15
Al_2O_3-CaO	16,17	MgO/SiO_2	18
Al_2O_3-CaO-MgO	19	MgO/SiO_2/Al_2O_3	29
Al_2O_3-CeO_2	20	$MgCO_3$	5
Al_2O_3-La_2O_3	20,8,21	La_2O_3	22
Al_2O_3-MgO	20,19	Nb_2O_5	23
Al_2O_3-MnO	24,25	SiC	26
$MgAl_2O_4$	27	SiO_2	28
Al_2O_3-SiO_2	29	SrO	30
BaO	30	SrO-SiO2	31
C	32,33	TiO_2	34,11,32,33
CaO	30	ZnO	34
CeO_2	35	ZrO_2	35
ZrO_2-CeO_2	35,36,37	Zeolite	38
MgO	12,30, 32,33,		

The mechanism for CH_4 adsorption and dissociation on transition metal surface has been claimed to be both directed [39] and precursor mediated [40]. Studies of the interaction of CH_4 with a Ni(111) surface suggested that in order to dissociate, CH_4 must be distorted from it tetrahedral shape to form a trigonal pyramidal structure, after which tunnelling of an H atom through the activation barrier occurs [1]. Nevertheless, neither a quantitative model nor a general consensus exists concerning the mechanism for CH_4 adsorption and dissociation on transition metal surfaces. It has been proven that CH_4 decomposition preferentially occurs on small Ni crystallites, and that the structure sensitivity of CH_4 dissociation on Ni surfaces, along with activity decrease is in the order of Ni(110)> Ni(100)> Ni(111) [1]. It was suggested that CH_x fragments are more likely to locate at a site on the metal surface which completes its tetravalency [1]. It is also observed that different CH_x species during the adsorption of hydrocarbons formed on different Ni catalysts and concluded that CH_x intermediates with lower values of x were more likely to form carbonaceous deposits [1].

The stepwise adsorption of CH_4 and then its decomposition into CH_x fragments on a metal surface are shown as follows [1]:

$$CH_4 + 2M \rightleftharpoons CH_3\text{-}M + H\text{-}M \quad (6)$$

$$CH_3\text{-}M + 2M \rightleftharpoons CH_2\text{-}M_2 + H\text{-}M \quad (7)$$

$$CH_2\text{-}M_2 + 2M \rightleftharpoons CH\text{-}M_3 + H\text{-}M \quad (8)$$

$$CH\text{-}M_3 + 2M \rightleftharpoons C\text{-}M_4 + H\text{-}M \quad (9)$$

where M_n is an ensemble of n surface metal atoms. This mechanism demonstrates the high probability of structure sensitivity in the formation of surface carbon because of the large ensemble of metal atoms needed.

The decomposition of CH_4 on supported transition metals has been studied extensively. In general, the decomposition yields surface carbon, H_2, C_2H_6, and C_2H_4 [27]. In DRM, CO and H_2 are major components in the effluent mixture. The CO comes from both CH_4 and CO_2. Thus, it seems plausible that during CO_2-CH_4 reforming, CH_x species formed on a transition metal surface may react with either oxygen species or hydroxyl groups, generated via dissociative adsorption of CO_2, on the support to yield CO and H_2 [1].

It is generally accepted that CO_2 chemisorption and dissociation on a transition metal surface is dominated by electron transfer and requires the formation of an anionic CO_2^- precursor , and CO_2 activation is reported to be structure sensitive [1].

As mentioned earlier, the origin of inactive carbon during DRM may occur via either CH_4 decomposition or CO disproportionation. CO disproportionation is exothermic; thus, the equilibrium constant decreases with increasing temperature. Conversely, CH_4 decomposition is endothermic; thus the equilibrium constant increases with increasing temperature. The calculation illustrates that for any reaction mixture of H_2, CO, H_2O, CO_2, and CH_4 at thermodynamic equilibrium, the extent of graphitic carbon deposition during reforming decreases at higher reaction temperatures, in agreement with experimental observations reported in the literature [1]. This would suggest that the main contributor to carbon deposition is CO disproportionation. CO dissociation on transition

metal surface is initiated via adsorption at a multiple coordinated site [1]. This adsorbed CO species then proceeds through a bent transition state lying essentially parallel to the surface prior to dissociation [1]. After dissociation on Ni, for example, subsequent CO adsorption on the C/Ni surface induces migration of carbon to subsurface Ni layers [41]. These adsorbed carbon atoms induce local reconstruction of the Ni surface, thereby lengthening nearby Ni-Ni bond and permitting a deeper carbon penetration into the Ni lattice [1]. At this point, carbon diffusion through the metal lattice may occur until the carbon atoms deposit in eventual graphitic layers on the back side of the metal crystallite. It has been suggested that carbon atoms, formed by CH_4 decomposition on the (100) and (110) Ni surfaces, diffuse across the Ni particle surface and by deposition on the (111) surfaces form ordered graphite layers aligned parallel to the metal–carbon interface [42]. The driving force for carbon diffusion in this process has been assumed to be a carbon concentration gradient.

To evaluate the effect of promoters and supports, modifications to the support, as shown in Table 2.1, have been investigated. It was observed that carbon deposition is suppressed when the metal is supported on a metal oxide with strong Lewis basicity [43]; i.e., increasing Lewis basicity of the support increases the ability of the catalyst to chemisorb CO_2 [1,16,25]. Increasing the concentration of adsorbed CO_2 reduces carbon formation via CO disproportionation by shifting the equilibrium concentrations. However, Tang et al. [19], and Zhang et al. [44] illustrated that the addition of MgO or CaO to Ni/Al_2O_3 greatly increased both catalyst activity and carbon deposition during CO_2 reforming of CH_4. Attempting to clarify the issue of carbon deposition during CO_2 reforming of CH_4, Swaan et al. [45] and Tsipouriari et al. [46] independently used

isotope labelling and temperature programmed oxidation (TPO) to reveal the carbon deposition mechanism. They found that carbon deposition initiated from both CH_4 and CO_2, but that from CH_4 is not dominant.

It is also plausible that carbon deposition is more closely related to the catalyst structure. For example, Chen et al. [47] studied DRM over Ni/Al_2O_3 and showed that carbon deposition is markedly suppressed if $NiAl_2O_4$ is formed during the pretreatment procedure. The difference in apparent activation energies for the reduction of NiO (18.1kJ/mol) and $NiAl_2O_4$ is indicative of relative strengthening of the Ni-O bond in $NiAl_2O_4$. This strong interaction results in the formation of primarily small Ni crystallites on the catalyst surface, which are relatively stable toward sintering and carbon formation. Prior to the study of this spinel structure, the improved performance of solid solution of NiO-MgO, which included extended activity maintenance at high conversion and the absence of carbon deposition had been reported [1]. Since then, investigations of CO_2-CH_4 reforming over Ni/MgO catalysts by Fujimoto and co-workers [12], Bradford and Vannice [32,33], and Ruckenstein and Hu [48] have provided additional evidence that NiO-MgO solid solutions can stabilize small Ni crystallites and enhance catalyst lifetime by decreasing carbon formation. The structure sensitivity of carbon deposition on Ni crystallites during CO_2-CH_4 reforming has been addressed recently, and on the basis of their transmission electron microscopy (TEM), thermal gravimetric analysis (TGA), TPO, and temperature programmed hydrogenation (TPH) experiments, Kroll et al. [28] concluded that faceted and flat particles produce little or no filamentous carbon, whereas small, spherical particles produce encapsulating

carbon. Oh-Shim Joo et al. [49] observed that the amorphous carbon could cover all the active metal sites and that the filament carbon does not cover the active metal.

Several recent investigations of supported Ni [11,12] catalysts have shown that carbon deposition can be greatly suppressed when TiO_2 or MgO is used as the catalyst support. As mentioned earlier, DRM more preferentially occurs on small Ni particles than the carbon formation reactions. The decomposition of CH_x requires large assembles of metal atoms. When TiO_2 or MgO is used as the support, it is helpful to form well dispersed and small Ni particles on the surface of catalysts. The SMSI effect facilitates the elimination of large ensembles of nickel on the surface of TiO_2 based catalyst [50] and a solid solution formed in the MgO based catalyst which induce very small active sites during the activation of the catalyst [12]. TiO_2, a support with the back spill-over property, can also influence the carbon deposition behaviour on the surface of active metals. TiO_2 can act as an O donor, from which O atoms will spill back to the surface Ni atom, which is acting as an O acceptor. The back spilled O can react with the carbon formed on the surface of the catalysts or the decomposed CH_x so as to suppress the carbon formation.

In order to remove the deposited carbon on the Ni/α-Al_2O_3 catalyst, L. Mleczko initiated the integration of fluidized bed reactor into syngas production [51]. Combustion of deposited carbon from the surface of catalysts can not only expose the active sites to the reacting molecules but also provide certain heat to sustain this high endothermic reaction. However, it was found that the unreduced catalyst had significant lower activity than the reduced catalyst [52]. So the external catalyst regeneration might be

necessary. In addition, the problem of metal dusting due to the high CO content in the reformed gas has to be taken into account with respect to the construction of the reformed gas boiler. These concerns make the development of a catalyst with low carbon deposition more attractive.

In summary, it appears that both CH_4 decomposition and CO disproportionation can contribute to the formation of inactive carbon deposits during DRM, with the relative contribution of each depending on the reaction conditions. Available data indicate that carbon formation is dependent on several parameters, such as the metal, metal crystallite structure, metal–support interactions, support acidity and basicity. Although the precise mechanism by which the dissociative adsorption of CH_4 occurs on a metal surface is unknown, it is reasonable to expect that CH_4 decomposition is dependent on the properties of geometric structure of the metal surface, and it is very likely to be a structure-sensitive reaction. Dissociation of CH_4 under CO_2-CH_4 reforming conditions yields a distribution of CH_x species that depends on both the metal and the support.

Two types of carbon can form during the DRM, amorphous and filament carbon. The amorphous carbon can encapsulate the Ni crystallite to deactivate the catalyst and the filament carbon can grow without significant influence on the activity of the catalyst. Sinter of Ni crystallite may also deactivate the catalyst. Supports which may interact or form solid solution with Ni can stabilize the Ni crystallites from carbon deposition and sintering.

2.3 Catalysts Preparation

In practice, different catalyst preparation methods have been used to adjust the structure of supports. Consequently, physical and chemical properties of the catalysts are modified. As discussed formerly, the status of the existence of Ni in the catalyst, the particle size of Ni, and the environment of the Ni particle have great effect on the performance of the catalyst. Ni catalyst prepared by different methods has demonstrated different activity and stability, as shown in Table 2.2. Wet impregnation [12], co-precipitation [12,53], sol-gel [6,36], and their combinations of these methods [54] are mostly reported. Some other methods [55,56] were also found in literature.

Tomishige et al. [12] investigated the Ni/MnO_2 catalyst prepared by co-precipitation and impregnation methods. The co-precipitated solid solution catalyst containing low nickel load has shown low carbon deposition for 3000h of time on stream, attributing to the small nickel particles dispersed on the support which inhibits carbon formation. Comparing to the wet impregnated catalyst, the co-precipitated catalyst has shown comparable advantage in catalyst activity and life.

Tang et al. [6] investigated γ -Al_2O_3 based Ni catalyst made by different techniques. The catalyst by impregnating Ni onto sol-gel made γ-Al_2O_3 showed the highest activity and stability with the lowest coke deposition. The catalyst made by sol-gel had compatible activity and stability. However, the catalyst made by impregnating Ni onto the commercial γ-Al_2O_3 demonstrated the poorest performance and the reactor was plugged within 3.5h by the formed carbon.

Table 2.2. Performance of catalysts made by different methods

Catalyst	Preparation method	Activity	Carbon Formation	Time on Stream (h)	Reference
Ni0.03Mg0.97O	Coprecipitation	240^{R}	0.05^{CR1}	3000	12
3mol% Ni/MgO	Impregnation	138^{R}	0.15^{CR1}	240	12
10wt% Ni/γ-Al_2O_3	Impregnation	N/A	0.095^{CR2}	3.5	6
10wt% Ni/γ- Al_2O_3	Sol-gel	N/A	0.003^{CR2}	N/A	6
10wt% Ni/γ- Al_2O_3	Sol-gel + Impregnation	N/A	0	80	6
Ni/ Al_2O_3	Sol-gel	N/A	low	60	13
8wt% Ni/TiO_2	Impregnation	N/A	Very low	110	11

^{R}: Reaction rate (μmol.g^{-1}.s^{-1}), ^{TO}: Turn over frequency (s^{-1})

^{CR1}: Carbon deposition rate (μmol-C. g^{-1}.s^{-1}), ^{CR2}: Carbon formation rate (g-C.g-cat^{-1}.h^{-1})

Hwang et al. [55] applied the supported Ni catalyst with the pillared clay base to DRM. It was found that the structure and properties of supports obtained by this method affected carbon deposition behaviour on the surface of the catalyst [53,55].

In conclusion, catalyst preparation method has shown significant effect on inhibiting carbon formation and stabilizing the Ni crystallites. Co-precipitation and sol-gel methods, which can promote the interaction between precursors, have shown better suitability for the catalysts for DRM than wet impregnation method.

2.4 Catalyst System Selection

In this thesis work, Ni-Ti system was chosen to be investigated. The catalyst was made using sol-gel method. The initiative was based on the following reasons.

First, although noble metals have shown superior performance to the Ni catalysts, the wide availability and cheap price of nickel make the latter more attractive.

Second, various researches have demonstrated that TiO_2 supported Ni catalyst posses good stability and lower carbon formation rate as shown in Table 2.2. It was concluded that the low carbon formation rate was due to the SMSI effect between TiO_2 and Ni. The SMSI effect facilitates the formation of small active sites. It can not only inhibit the carbon formation but also stabilize the Ni crystallite.

Third, the sol-gel method provides close reaction between precursors and has the nature to improve interaction between them. As shown in the previous part, the sol-gel made

catalysts have shown better performance than the wet impregnation made catalysts for DRM. The sol-gel made Ni-Ti catalyst has shown good activity and stability for other reactions [9].

2.5 Sol-gel Method

The sol-gel method is a versatile solution process for making ceramic, glass materials, and catalysts. In general, the sol-gel process involves the transition of a system from a liquid "sol" (mostly colloidal) into a solid "gel" phase. Applying the sol-gel process, it is possible to fabricate ceramic or glass in a wide variety of forms: ultra-fine or spherical shaped powders, thin film coatings, ceramic fibres, microporous inorganic membranes, monolithic ceramics and glasses, or extremely porous aerogel materials. The starting materials, known as precursors, used in the preparation of the "sol" are usually inorganic metal or metal compounds. The most obvious precursors are molecules having already metal-oxygen bonds, namely metal alkoxides M(OR)n or oxoalkoxides $MO(OR)_n$ (R= saturated or unsaturated organic group, alkyl or aryl). At its simplest level, sol-gel chemistry with metal alkoxides can be described in terms of two classes of reactions:

Hydrolysis: $\text{-M-OR} + H_2O \longrightarrow \text{-M-OH} + \text{ROH}$ (10)

Condensation: $\text{-M-OH} + \text{XO-M-} \longrightarrow \text{-M-O-M-} + \text{XOH}$ (11)

where X can be either H or R (alkyl group).

Such a description oversimplifies the overall process because it does not correctly represent the molecular formulas of the intermediates and end products, nor does it depict the simultaneous occurrence of the two reactions. However, this

oversimplification captures the key phenomenological idea that a three-dimensional gel network comes from the condensation of partially hydrolyzed species.

The main advantages of sol-gel techniques for the preparation of materials are low temperature of processing, versatility, flexible rheology allowing easy shaping and embedding. This technique has been widely employed in catalysis field. The most important characteristic of the sol-gel preparation of catalytic materials is its ease of control that translates into the following advantages:

(1) the ability to maintain high purity (because of purity of starting materials);
(2) the ability to change physical characteristics such as pore size distribution and pore volume;
(3) the ability to vary compositional homogeneity at a molecular level;
(4) the ability to prepare samples at low temperatures;
(5) the ability to introduce several components in a single step;
(6) the ability to produce samples in different physical forms.

Factors that influence the properties of final products prepared using sol-gel technique include hydrolysis ratio, acidity of the hydrolysant, gelation condition, drying condition and procedures, and solvent property.

Hydrolysis ratio, H, defined as the moles of water per mole of metal alkoxide, $M(OR)_m$, is considered one of the most important influential factors on the properties of the sol-gel made composite. When $H<1$, infinite network seldom forms due to the low functionality of the precursor towards condensation. Few M-OH groups are available for

cross-linking gelation or precipitation when there is no local excess of water. When 1<H<m, polymeric gels can form. And when H>m, cross-linked polymers, particulate gels, or precipitates can form due to the existence of excess amount of water.

pH value, usually the acidity of the precursor solution or hydrolysant (AC) affects the gelation time, defined as the time it takes for a solution to undergo a rapid rise in viscosity that corresponds to the transition from a viscous fluid to an elastic gel. This effect may improve the cross-link of precursors so as to result in a better porous structure. It has been found that an acidic precursor solution promotes the formation of small metal crystallites [57].

Gelation is a complex process that may combine a number of physical and chemical sub-processes. Varying gelation temperature effectively alters the relative rate of these competing processes. Solvent can change the nature of an alkoxide through solvent exchange or affect the condensation reaction directly.

Drying process affects the porous structure due to the different extent to which the original structure is destroyed in the removal of solvent from it. Materials dried by different techniques are named differently. Aerogel means the composite dried in the supercritical solvent medium. This drying process preserves the fine porous structure developed during the gelation by reducing the surface tension between the solvent and the solid. Xerogel is given to the composite after conventional drying by heating the material in air, where the structure of micropores cannot be preserved. So some solvent with low surface tension may help xerogel to preserve the porous structures. Calcination

procedure can also greatly affect the surface area of the sol-gel made composite. It was reported [9] that the Ni-Ti aerogel heated at 1K/min posses much higher surface area than the one heated at 5K/min.

2.6 Objectives of the Work

This thesis work is to prepare Ni-Ti catalysts which are stable for the DRM using sol-gel method. To develop an industrially usable catalyst, the following requirements have to be met. First of all, the raw material must be available and relatively cheap. Secondly, the preparation process should be as simple as possible. Thirdly, the catalyst must have acceptable activity, selectivity, and stability. Literature review has shown that nickel is one of the cheapest metals which are active for DRM and that the sol-gel made Ni-Ti catalyst would mitigate carbon formation and thus facilitate longer catalyst life. However, the performance of Ni-Ti sol-gel made catalyst needs to be evaluated with DRM at higher temperature around 900 to 1000K. If the Ni-Ti catalyst wouldn't reach the expectation, some adjustment to this system should be conducted.

The research work is planned as follows:

1. Because surface area is a very important property for catalyst and calcination temperature has significant effect on the final surface area of sol-gel made catalysts, two important parameters of sol-gel synthesis, the hydrolysis ratio and the hydrolysant acidity, will optimized in terms of the surface area of the catalyst. Then the effect of calicination temperature on surface area and pore size will be studied.

2. Instrumental analyses such as X-ray diffraction (XRD), X-ray photoelectron spectroscopy (XPS), TG/DTA, scanning electron microscopy (SEM) and TEM will be

used to characterize both surface and bulk properties so as to further understand the impact of sol-gel processing and calcination conditions on the catalyst properties.

3. The reduction of catalyst will be studied and the optimal catalyst reduction condition such as reduction temperature, reduction time in terms of catalyst activity will be determined.

4. The effect of feed gas flow rate and reaction temperature will be evaluated in terms of catalyst activity, selectivity and stability for DRM reaction.

5. Adjustment to the Ni-Ti system by adding the third component to improve the catalyst activity and stability will conducted when necessary.

CHAPTER 3

EXPERIMENTAL DESCRIPTIONS

3.1 Catalyst Preparation

The catalysts used in this study were prepared by sol-gel method. The precursors were $Ni(NO_3)_2 \cdot 6H_2O$ (98%, Lancaster, Lancaster Synthesis Inc., Pelham, NH) or $Ni(Ac)_2.6H_2O$ (99+%, Alfa Aesar, A Johnson Mathey Company, Ward Hill, MA), $Ti(BuO)_4$ (99+%, Alfa Aesar, A Johnson Mathey Company, Ward Hill, MA) and $Al(NO_3)_3.9H_2O$ (>98%, EMD, Gibbstown, NJ). MeOH (>99.9%, Burdick & Jackson, Muskegon, MI) was used as the solvent for both the precursors solution and the hydrolysant. The molar ratio of Ti/MeOH in the precursor solution was kept at 0.12. Hydrolysis process was catalyzed by HNO_3 (69-70%, EMD Chemicals Inc., Gibbstown, NJ). For every batch of preparation, the amount of each reactant was calculated in order to obtain 10g of catalysts. The hydrolysant was made of proper amount of distilled water, nitric acid and 20mL MeOH. The Ni load was 10wt% for all catalysts during the sol-gel optimization, where the Ni load is defined as weight percent of elemental Ni in the catalyst. Catalysts with different Ni load, varied from 1wt% to 10wt%, for the activity and stability evaluation were prepared under the determined condition.

The catalyst preparation procedure is described below. Required amounts of $Ti(BuO)_4$ and $Ni(NO_3)_2 \cdot 6H_2O$ were dissolved in MeOH (Recipe of each run is shown in Appendix A). The transparent green solution was stirred for 24h in a covered flask for a thorough reaction between precursors. The hydrolysis of the alkoxide solution was carried out in a covered flask. The hydrolysant was added drop wise into the alkoxide solution (the recipes of hydrolysants are also shown in Appendix A) under strong stirring. A green bouncy transparent gel was formed shortly after the addition of hydrolysant. The formed gel was aged in the sealed flask for 24h, and then dried in ambient condition at 453K for 10h. The dried catalyst was calcined in air at 573K for 24h. Selected samples were calcined in air at 773K and 973K for 24h respectively. Catalysts were dark grey after calcination below 773K and were bright yellow after calcination at 973K. The catalysts after calcination at 973K were denoted as xwt% Ni-Ti, where x represents the value of Ni load of the catalyst.

For the preparation of aluminium integrated catalyst, the required amount of $Al(NO_3)_3.9H_2O$ was added into the well mixed $Ti(BuO)_4$ and $Ni(NO_3)_2.6H_2O$ solution in MeOH. A green colloidal suspension formed after the addition of $Al(NO_3)_3.9H_2O$ since the crystal water from $Al(NO_3)_3.9H_2O$ was sufficient for the partial hydrolysis of Ti^{4+}. The colloidal mixture was kept under inert protection for 24h before the hydrolysant made with the above mentioned recipe was added to obtain thorough hydrolysis. No firm gel had formed after stirring for 24h. The thick colloidal was calcined at 1023K for 10h with a ramp rate of 1K/min from 298K. The catalyst was bright green after the

calcination The aluminium integrated catalysts were denoted as x wt% Ni-Ti_y-Al_z, where x, represents the Ni load of the total weight of the catalyst, y and z represent the weight ratio of TiO_2 and Al_2O_3, respectively, and y+z=1. For the temperature programmed reduction (TPR) analysis, pure NiO was made by calcining $Ni(NO_3)_2.6H_2O$ at 973K for 10h.

3.2 Sol-gel Optimization Process

Dispersability of active metal on surface of catalyst is crucial in determining the activity. Materials with large surface area can disperse the active metal evenly. Thus, the specific surface area (SA) is a very important property for catalyst. Large surface area comes from rich porous structure. On the other hand, in sol-gel method, hydrolysis ratio and acidity are two of the process parameters that affect the final surface area and porous structure. Therefore, it is necessary to find out the optimum H and AC that are able to produce large surface area and rich porous structure. In thiswork, Design Expert 6.0, developed by Stat-Ease, a Windows-based software, was used to design the experimental plan that would determine the optimum H and AC. Then, experiments were carried out according to this plan.

Total 13 runs were required by the software (shown in Table 3.1). The hydrolysis ratio was varied from 1 to 6 and the acid/alkoxide was in the range of 0.05 to 0.35. Two response factors were BET surface area (m^2/g) and average pore diameter (nm). Five runs at the central point, H=0.35 and AC=0.2, were required to evaluate the reproducibility of sol-gel process.

Table 3.1. Experimental design using Design Expert®

Standard	Run	Hydrolysis ratio	Acid/alkoxide
2	1	5.27	0.09
5	2	1	0.2
13	3	3.5	0.2
7	4	3.5	0.05
10	5	3.5	0.2
6	6	6	0.2
3	7	1.73	0.31
12	8	3.5	0.2
8	9	3.5	0.35
4	10	5.3	0.31
1	11	1.73	0.09
11	12	3.5	0.2
9	13	3.5	0.2

3.3 Catalyst Characterization Techniques

In order to understand the changes in both chemical and physical properties and structure of the catalysts during the preparation and pre- or post-reaction, the following instrumental analyses were applied.

3.3.1 BET Analysis

The BET surface area (SA) and pore distribution were measured by N_2 adsorption at the temperature of 77K using Micromeritics ASAP 2000. Around 0.5g catalyst was used for each analysis. The degassing temperature was 473K to remove the moisture and other adsorbed gases from the catalyst surface. The sample tube was evacuated to 20μmHg during the analysis.

3.3.2 Temperature Programmed Reduction

The reduction behaviour of catalysts was studied by TPR with the CHEMBET-3000. Around 0.1g catalyst was used for each analysis. The loaded sample tube was placed in the middle of a furnace and heated at a rate of 10K/min from room temperature to 1273K. A gas mixture of H_2(3%)/N_2 continuously flowed through the catalyst bed at a rate of 30NmL/min. The whole process was controlled by the software and the data were collected automatically.

3.3.3 Thermogravity/Differential Thermogravity Analysis

The thermal behaviour of pre- and post-reaction catalysts was studied using TG/DTA analysis. The data were obtained by a PerkinElmer, Pyris Diamond TG/DTA equipment.

Air continuously flowed through the sample holder during the process. The platinum sample holder was fully loaded after the equipment was balanced. The temperature was increased from 303K to 1223K at a rate of 5K/min. The data were collected automatically by the software.

3.3.4 X-ray Diffraction

The crystalline structure of catalysts was studied using XRD analysis. The diffraction patterns were obtained by a Rigaku/Rotaflex Cu rotatory anode equipment with a generator voltage of 40V and tube current of 40mA. For the preparation of the sample, catalyst was grounded into powder and mixed with methanol to form a mud. The mud was loaded to the coarse side of a glass plate and placed under ambient condition for drying. The dried sample plate was then loaded in the analysis chamber. Each sample was scanned at a rate of 7^{o}/min. The 2θ, also denoted as 2 Theta, was varied from 10 to 90^{o}.

3.3.5 X-ray Photoelectron Spectroscopy

The composition and oxidation status of surface components of the catalysts were studied using XPS analysis. The spectra were obtained using an Axis-165 spectrometer (Kratos Analytical) at room temperature with an Al-Kα radiation source. The initial photon energy was 1486.71eV at the operation power of 210W. For the survey spectra, the pass energy was 160eV with a binding energy range 0-1,100eV and a step of 0.33eV. For the high resolution spectra, the pass energy was 20eV and the step was 0.1eV.

3.3.6 Scanning Electron Microscopy

The surface particle property of the catalysts was studied using SEM analysis. The SEM was conducted using a Philips SEM 505 instrument at a voltage of 30kV. The powdered sample was loaded onto a copper sample plate. Before the analysis, the sample plate was coated with gold to form a conductive layer.

3.3.7 Transmission Electron Microscopy

The bulk particle property of catalyst was studied using TEM (Philip CM10). For the preparation of the sample grid, the catalyst was grounded into fine powder and dissolved in water. A very small drop of water with suspended particles was dropped onto a copper grid coated with a layer of polyethylene. The grid was loaded into the sample chamber after it was dried. The analysis was conducted under high vacuum.

3.4 Catalyst Evaluation

The schematic of the reactor system is shown in Figure 3.1. The feed gases are supplied from cylinders and the flow rate of each gas is controlled by a mass flow controller (MFC) (Read Out & Control Electronics 0154, Brooks Instrument). The feedstock is mixed in a mixer before entering the reactor. Mixer, preheater, and furnace are enclosed in a bench top reactor system (BTSR-jr, Autoclave Engineers, Erie, PA). The furnace is put in a well insulated box which can be heated up to 523K to preheat the feed gases. The temperature of the pre-heater is controlled by a temperature controller (2132, EURITHERM). The temperature of the furnace is controlled by a temperature controller (2416, EURITHERM) which has 8 segments. The temperature of the catalyst bed is read

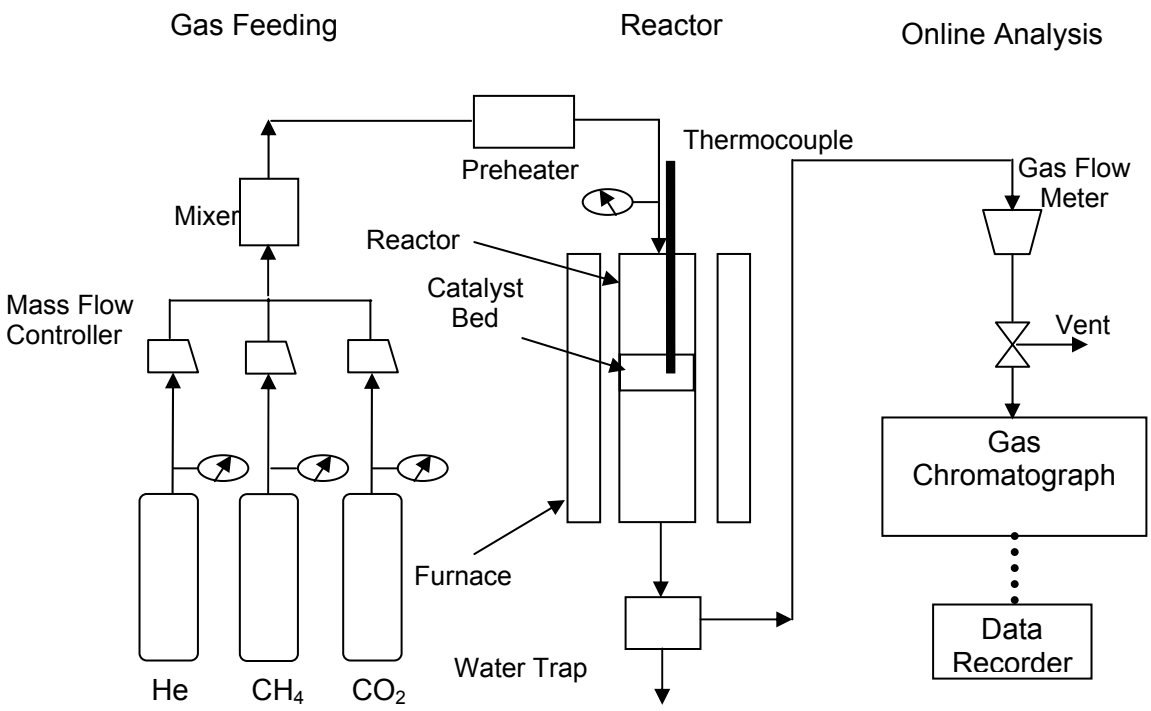

Figure 3.1. Schematic diagram of the reactor system.

out by an indicator (2132, EURITHERM). A quartz tube with an innner diameter of 5.6mm, external diameter of 9.5mm and length of 255mm (Autoclave Engineers, Erie, PA) was used as the reactor. Both ends of the tube were connected with the inlet and outlet tubes, respectively, using SwageLog fittings and graphite ferrules (Autoclave Engineers, Erie, PA). A safety valve is installed before the quartz tube reactor which could open once the pressure was over 7psig so as to protect the quartz reactor. Moisture in the effluent can be trapped down by an ice bathed water trap. However, in this research, no significant amount of water was observed and this trap wasn't used. A 6890N gas chromatograph (GC) (Agilent Technologies) equipped with a thermal conductivity detector (TCD) is used to analyze the effluent gas on line. All effluent gases were discharged into vent.

0.5g catalyst (0.25g for the Ni-Ti-Al catalyst) (45-80 Mesh) diluted with 0.5g quartz sand (45-60 Mesh) was packed in the reactor for each run. The catalyst bed with a length of about 2.2cm was supported by quartz wool. The position of catalyst bed in the tube was measured to ensure that it was located in the middle section, generally considered as an isothermal section, of the furnace. A thermocouple was inserted from the top of the tube into the middle of the catalyst bed. The reaction was operated under atmospheric pressure and at 973K. Before the DRM reaction, the catalyst was reduced in-situ with a mixture of H_2/N_2 in 30/60 SCCM/min at 973K for 2h. H_2 then was turned off and N_2 was allowed to flow through the catalyst bed for another 0.5h. The furnace temperature was increased to 988K for the reaction. The feed gases, with the ratio of CH_4:CO_2:N_2 in 1:1:1.8 were introduced at a WHSV from 10,000 to 90,000$cm^3g^{-1}h^{-1}$ through the catalyst bed. All the gases were supplied by PRAXAIR (PRAXAIR Canada

Inc., Mississauga, ON) and the purities of CH_4, CO_2, N_2, H_2, were 99.2%, 99.9+%, 99.9+%, and 99.9%, respectively.

A GS-GASPRO capillary column (J&W Scientific) with 60m in length and 0.32mm in inner diameter was employed to separate the effluent components. Helium (Ultra high purity 5.0, PRAXAIR Canada Inc., Mississauga, ON) was used as the carrier gas. In order to separate CO from N_2 peak, the column needs to work at low temperature. Thus, a pressure relief valve is installed in the GC to introduce liquid CO_2 into the oven. An eductor tube is installed inside the cylinder by which liquid CO_2 can be drawn. A filter is installed between the cylinder and the relief valve to prevent fine particles from entering the GC. The sampling loop is controlled by an air powered 8-port valve. The on-line analysis is controlled by the HP ChemStation. The method for GC analysis was as follows: The oven temperature was kept at 213K for 3 minutes before ramping it to 303K at a rate of 25K/min, and then the oven was kept at 303K for 5 minutes. The column was operated under a constant pressure mode. The pressure of helium flow through the column was 20psig at a rate of 3.0mL/min and the outlet was at ambient condition. The average velocity of the helium flow was 35 cm/sec. The GC inlet was heated to 473K at a pressure of 20psig. A split flow mode was applied with a split ratio of 20:1. The total flow was 65.3mL/min. The sequences of gases coming out of the column are H_2, N_2, CO, CH_4, and CO_2. The GC signals were calibrated prior to the analysis of product gases. The calibrations are shown in Appendix A. The raw data of each run are given in Appendix B.

Chapter 4

Results and Discussion

4.1 Catalyst Preparation and Characterization

4.1.1 Effect of Hydrolysis Ratio and Acid/Alkoxide on Catalyst Surface Area and Pore Structure

13 runs were conducted according to the experimental plan developed by using the Design Expert software. Because the calcination temperature dramatically affects the SA and pore structure, relatively low calcination temperature (613K) was used for this part of the experiment so as to be able to observe the changes in SA and pore size distribution resulted from the change of H and AC. Table 4.1 shows the experimental results of the 13 runs in SA and average pore diameter, based on which two 3-D diagrams were generated by the Design Expert software. One is the quadratic relation between surface area and H, and AC (Figure 4.1) and the other is the linear relation between average pore diameter and H, and AC (Figure 4.2). Surface area of the sol-gel made Ni-Ti can reach at least $242m^2/g$. The highest surface area can reach around $300m^2/g$. Most pores distribute between the meso-pore range, 2-15nm. Statistic analysis by the software shows that the correlations are significant with a 95% confidence level. These effects can be explained qualitatively as follows:

Table 4.1. Effects of hydrolysis ratio and acidity on surface area and average pore diameter

Standard	Run	Hydrolysis ratio	Acid/alkoxide	SA (m^2/g)	AveragePore Diameter (nm)
2	1	5.27	0.09	299.7	3.71
5	2	1	0.2	281.3	2.20
13	3	3.5	0.2	260.8	3.34
7	4	3.5	0.05	294.5	3.03
10	5	3.5	0.2	250.2	3.48
6	6	6	0.2	281.4	3.16
3	7	1.73	0.31	275.6	2.64
12	8	3.5	0.2	256.1	3.31
8	9	3.5	0.35	278.3	3.11
4	10	5.3	0.31	262.7	3.36
1	11	1.73	0.09	242.1	1.94
11	12	3.5	0.2	250.6	2.81
9	13	3.5	0.2	261.4	2.77

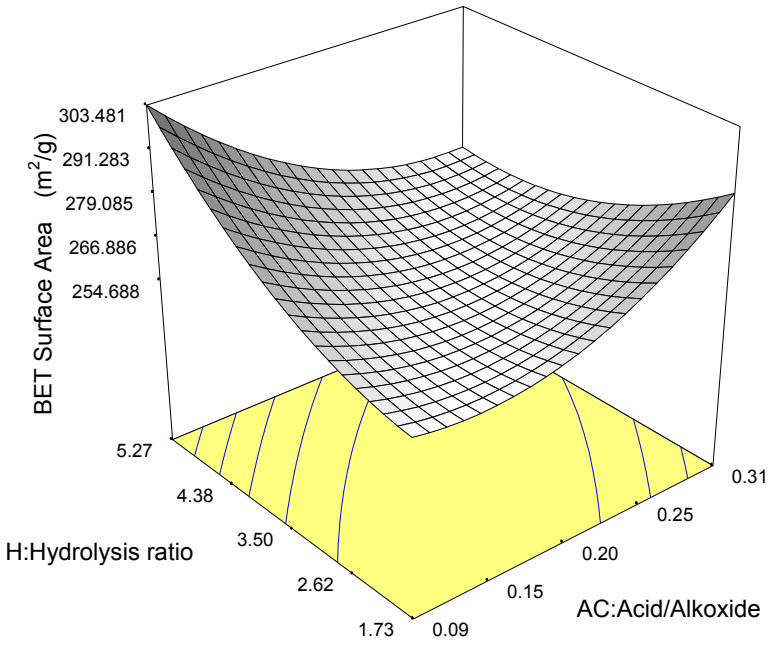

Figure 4.1. Chang of the BET surface area with H and AC of the sol-gel made Ni-Ti xerogel composite.

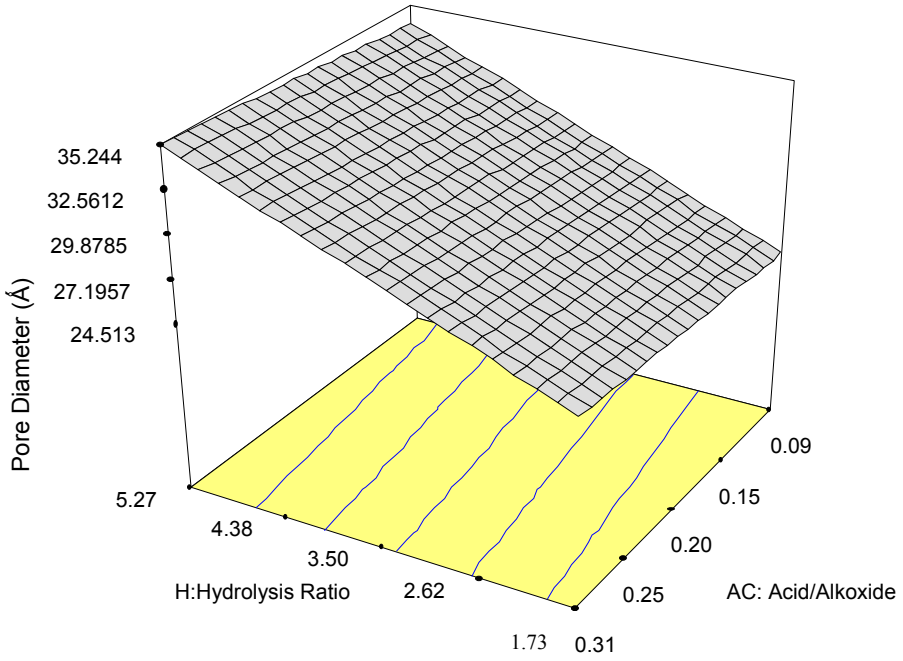

Figure 4.2. Change of the average pore diameter with H and AC of sol-gel made Ni-Ti xerogel composite.

Ti^{m+}, as a highly electronphilic functional group, can condensate very quickly once sufficient amount of OH^- were supplied. Typically, the following reactions take place during the hydrolysis and condensation:

$$\equiv Ti\text{-}OR + H_2O \rightleftharpoons \equiv Ti\text{-}OH + ROH \quad \text{(hydrolysis)} \tag{12}$$

$$\equiv Ti\text{-}OH + HO\text{-}Ti\equiv \rightleftharpoons \equiv Ti\text{-}O\text{-}Ti\equiv + H_2O \quad \text{(water condensation)} \tag{13}$$

$$\equiv Ti\text{-}OH + RO\text{-}Ti\equiv \rightleftharpoons \equiv Ti\text{-}O\text{-}Ti\equiv + ROH \quad \text{(alcohol condensation)} \tag{14}$$

Water condensation is completed before the alcohol condensation takes place due to electronic and steric effects [58]. At low AC, if insufficient water is supplied, i.e., $1<H<4$, alcohol condensation would occur after water condensation is completed. Two different condensation processes would lead to an inhomogeneous structure which is more vulnerable for the drying and calcination procedures. When H is larger than titanium coordination number, 4, only water condensation exists, leading to a homogeneous structure of the catalyst. Thus, more water supplied for the hydrolysis, more homogeneous and stable structure can be obtained. As a result, higher BET surface area can be obtained as H increased.

However, the application of acid catalyst greatly affects the gel rate and morphology of the final products [59]. When acid is present, different condensation reactions occur [59]:

$$\equiv Ti\text{-}OH + H_3O^+ \rightleftharpoons \equiv Ti^+ + 2H_2O \tag{15}$$

$$\equiv Ti^+ + HO\text{-}Ti\equiv \rightleftharpoons \equiv Ti\text{-}O\text{-}Ti\equiv + H^+ \tag{16}$$

When the solution is strong acidic, i.e., low AC and low H or high AC and low H, high concentration of H^+ in the solution keeps breaking down the interlayer bonds (Reverse reaction of reaction 16), leading to a monolayer structure. Consequently, a poor

networking structure would form, resulting in a relatively lower surface area. When excessive amount of water exists, i.e., high H and low AC, acid is diluted and the catalytic role is weakened. The fast water condensation reaction (Reaction 13), rather than reaction 16, is dominant. As discussed previously, the water condensation would lead to a homogeneous networking structure, resulting in a relatively larger surface area.

We were looking for a condition under which material with high surface area can be obtained, an optimal operation condition was desired. Table 4.1 shows this condition is at H=5.22 and AC=0.10 when other parameters such as temperature for hydrolysis , drying and calcination are fixed. It is realized that these temperatures, especially the one of calcination, would significantly impact the surface area. However, we assume that the optimized H and AC will give relatively higher surface area even at other calcination temperature. Therefore, the catalysts samples from now on would be prepared at H=5.22 and AC=0.10.

The BET results of two catalysts hydrolyzed under different temperatures (273K and 298K) but calcined at a higher temperature, 773K, are shown in Table 4.2. The catalyst geled under lower temperature posseses a higher surface area, but it took longer time to form a transparent gel because lower temperature slows down the hydrolysis rate. The prolonged gelation time facilitated the formation of polymerized structure. As a result, higher surface area was obtained. The two samples have the same pore volume but the lower gelation temperature leads to smaller pore diameters, which indicates a better porous structure. The average pore diameters of these two catalysts are 2.39 and 2.63 nm, respectively, and most pores are located in the meso-pore range. Although

Table 4.2. Effect of gellation temperature on surface area and porosity of Ni-Ti xerogel composite

Gel Temperature (K)	BET surface area (m^2/g)	Pore volume (cc/g)	Average pore diameter (nm)
273	182.2	0.11	2.39
298	161.5	0.11	2.63

(Other preparation parameters: H=5.22; AC=0.10; Drying temperature: 453K; Ni load: 10wt%)

continuing to lower the hydrolysis temperature may increase more in surface area, hydrolysis at room temperature gives much ease in preparation and thus is preferred.

4.1.2 Thermogravity and Differential Thermogravity Analysis

The TG/DTA pattern of the uncalcined xerogel catalyst is shown in Figure 4.3. The TG pattern shows an obvious weight drop from the starting point to 723K, due to the evaporation of moistures, methanol solvent, and BuOH generated during hydrolysis and the decomposition of nitrate. A steady horizontal TG line after 723K shows no further weight loss. In the DTA pattern, the negative peak at 373K indicates the occurance of an endothermic process, which is reasonablly attributed for the evaporation of moisture since the reaction temperature occurs below 473K. The first positive peak from 473 to 563K is related to the decomposition of nitrate. The second positive peak, which is broader than the first one, is associated with the decomposition of hydrocarbons which is derived from the the precursors or the couplings during the calcination. The broadness of the second peak indicates the complexity of the decomposition procedure of hydrocarbons. A steady horizontal DTA line after 723K indicates that the catalyst is thermally stable after calcination at 723K. However, DRM would take place at 973K. Therefore, the catalyst should be finally calcined at an equivalant or higher temperature to avoid any possible crystalline transformation during the reaction.

4.1.3 Effect of Calcination on Surface Area and Pore Structure

Specific surface areas, average pore diameter, and pore volume of catalysts calcined under different temperatures were presented in Table 4.3. The BET surface area of the catalyst is 426m^2/g after calcination at 453K. It dropped to 282, 81, and 2m^2/g as

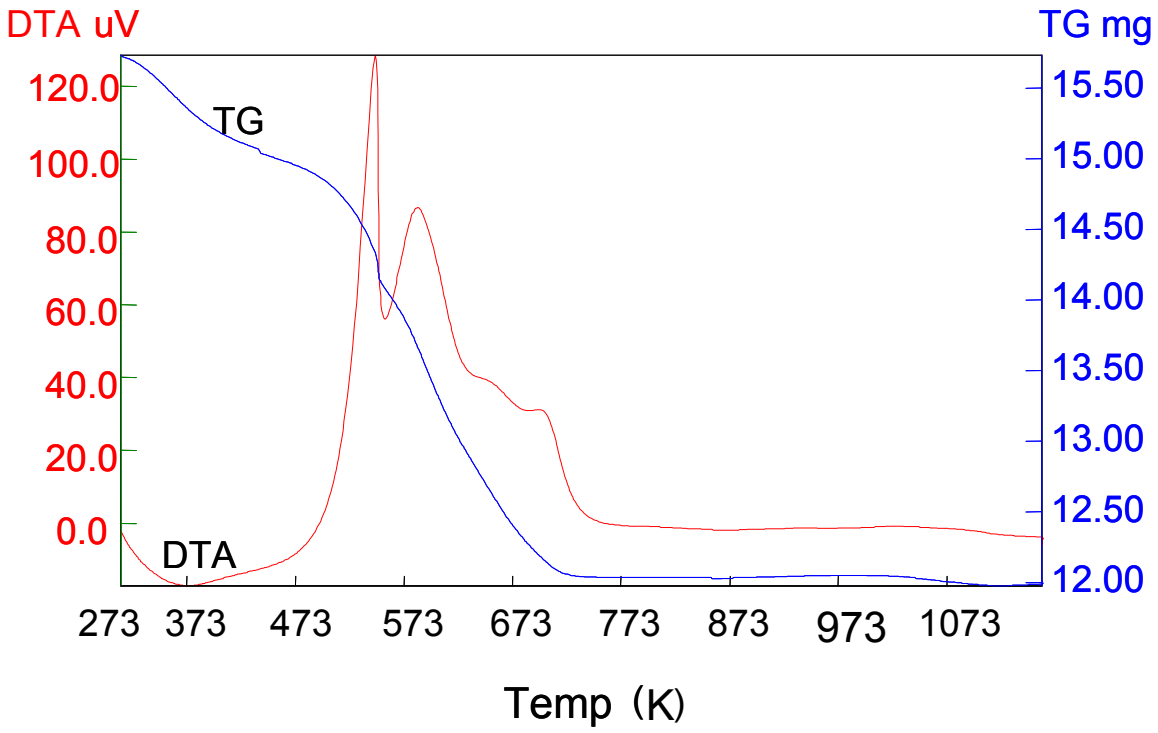

Figure 4.3. TG/DTA analysis of the uncalcined Ni-Ti composite xerogel catalyst.

(Other preparation parameters: H=5.22; AC=0.10; Hydrolysis temperature:298K;

Drying temperature: 453K; Ni load: 10wt%)

Table 4.3. Heat effect on the textural properties of sol-gel made Ni-Ti xerogel catalysts

Calcination Temperature (K)	Surface Area (m^2/g)	Average Pore Diameter (nm)	Pore Volume (mL/g)
453	426.1	2.1	0.22
613	282.4	3.3	0.24
773	81.5	6.2	0.13
973	1.9	15.3	0.01

(Other preparation parameters: H=5.22; AC=0.10; Hydrolysis temperature:298K; Drying temperature: 453K; Ni load: 10wt%)

calcination temperature increased to 613, 773, and 973K, respectively. The average pore diameter increases from 2.1 nm at 453K to 15.2nm at 973K. The results also show that the pore adsorption volume decreases as calcination temperature increases. It is obvious that higher temperature calcinations crushed the pore structure of the catalyst. The steady increase of average pore diameter indicates the loss of pores of relatively small diameter and the drastic decrease of pore adsorption volume indicates the loss of total amount of pore volume. It was observed that pore volume slightly increased from 0.22 to 0.24 as calcination temperature increased from 453 to 613K before it steadily dropped. This increase is due to the removal from the pores of nitrogen and carbon brought in by precursors.

As shown in Table 4.3, the surface area dropped to $2m^2/g$ and pore volume is very small as calcination temperature increased to 973K. It means that the porous structure of the sol-gel made catalyst is very sensitive to calcination temperature. A poor porous structure of the catalyst directly leads to its poor surface area. Lee et al. [9] reported that aerogel catalyst could maintain high surface area when it was calcined under a strict temperature ramping, for example, 1K/min, and under inert protection, for example, keeping He or N_2 flowing through the whole calcination. However, such efforts for this project didn't prove that observation. Lee and coworkers also reported that if the catalyst was dried by low temperature CO_2 supercritical fluid, surface area as high as $49m^2/g$ could be maintained even when the catalyst was calcined at 973K. Drying the aerogel in supercritical fluid can reduce the damage to the porous structure by eliminating surface tension between liquid and vapour phases and it can help to remain

the whole gel structure intact. Because this project was to seek a simple catalyst preparation method, supercritical drying was not attempted. The xerogel showed a bright yellow color after calcination at 973K, indicating the formation of nickel titanate [11].

4.1.4 Effect of Calcination on Crystallite Structure

Figure 4.4 shows the XRD patterns of the catalysts calcined at different temperatures. It is observed that the catalyst is still amorphous after calcination at 573K. Crystallization starts at 673K and small amount of brookite titania (Br) was observed. The amount of titania crystallite grew and nickel titanate began to form at 773K. The peaks became more intensive as calcination temperature increased. After the catalyst was calcined under 973K for 10h, only small amount of brookite (TiO_2) can still be observed, and most TiO_2 has transformed into the form of rutile (R). Nickel titanate was the dominant phase and no bunsenite was observed during the whole calcination process. This is in agreement with the colour changes of the catalyst. Catalyst made by wet impregnation, with no presence of nickel titanate, is shown dark brown after calcination at 973K [11]. Though, in this project, the catalyst shows dark colour after calcination at 773K, yellow particles can be observed, which is a typical indication of the presence of nickel titanate [11]. The catalyst calcined at 873K is shown light yellow and that calcined at 973K is bright yellow.

It is worth noting that the peaks in pattern (d) are narrower compared to patterns in (c) and it is even narrower in pattern (e) in the XRD analysis. The decrease of peak width

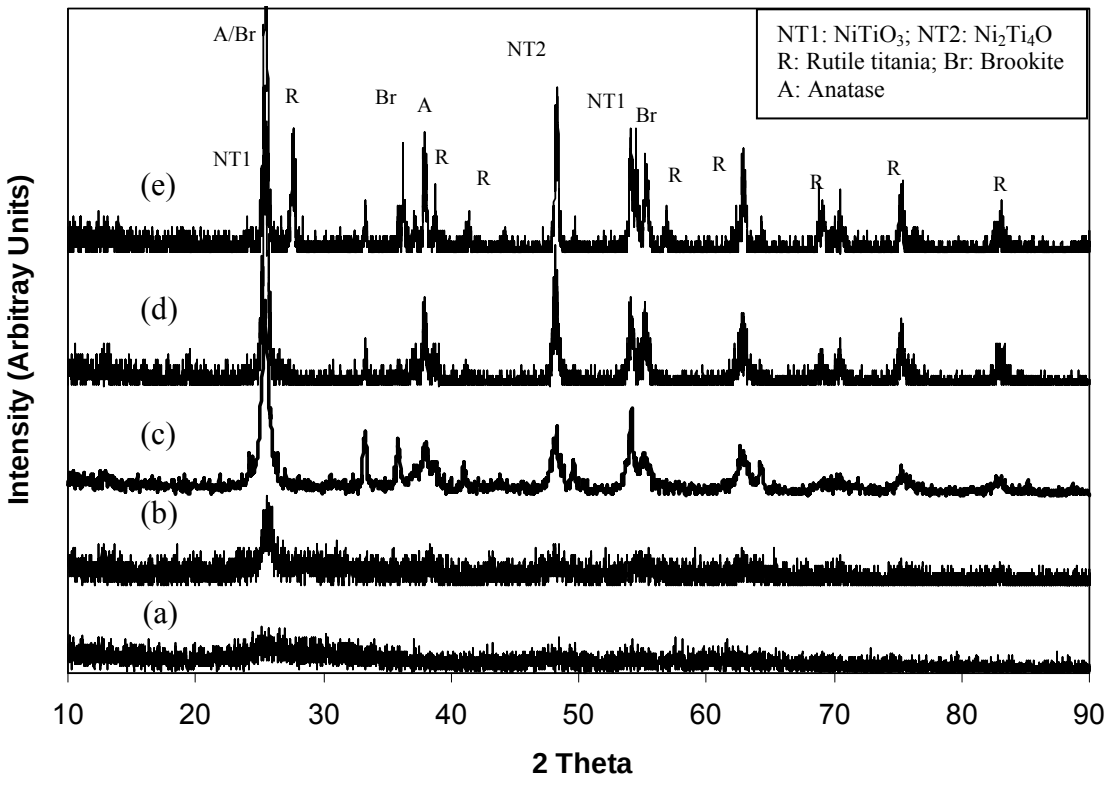

Figure 4.4. X-ray diffraction patterns of the Ni-Ti composite xerogel catalysts calcined at (a): 573K for 10 h; (b): 673K for 10 h; (c): 773K for 10 h; (d): 873K for 10 h; (e): 973K for 10 h.

(Other preparation parameters: H=5.22; AC=0.10; Hydrolysis temperature:298K; Drying temperature: 453K; Ni load: 10wt%)

indicates that the particles of both TiO_2 and nickel titanate grew up. This can well explain the phenomena of the decrease of BET surface area as calcination temperature increased. Lee et al. [9] reported that the Ni-Ti aerogel catalyst is still X-ray amorphous even after the calcination at 773K under an inert protection. In this study, crystallization of titania started at 673K, which may be due to the calcination in air. Three phases of titania were observed in this study rather than only rutile even after calcination at 973K. It was reported that, brookite, anatase, and rutile can coexist in the temperature from 673 to 973K [60] and anatase TiO_2 transforms to rutile between 903 and 973K [61]. The extension of the co-existing range of brookite, anatase, and rutile in this study may be due to the integration of Ni.

The TEM images (Figure 4.5) are in agreement with the XRD results. A large cluster was observed after calcination at 613K, indicating a good networking and amorphous structure of the material. After calcination at 973K, the big cluster crushed and divided into small particles with poor network. Some small particles which can be seen differently might be nickel titanate decorating on TiO_2, with an average particle size of 80nm. Those large particles might be the aggregated TiO_2 with an average particle size of 250nm. The aggregation of TiO_2 could decrease the dispersibility of Ni on catalyst so as to decrease its activity.

4.1.5 Effect of Calcination on Surface Composition

The catalysts with a Ni content of 4wt%, which conresponds a bulk Ni/Ti ratio of 0.042, were analysed using XPS. The elements detected on the surface were Ti, Ni, O, C and N,

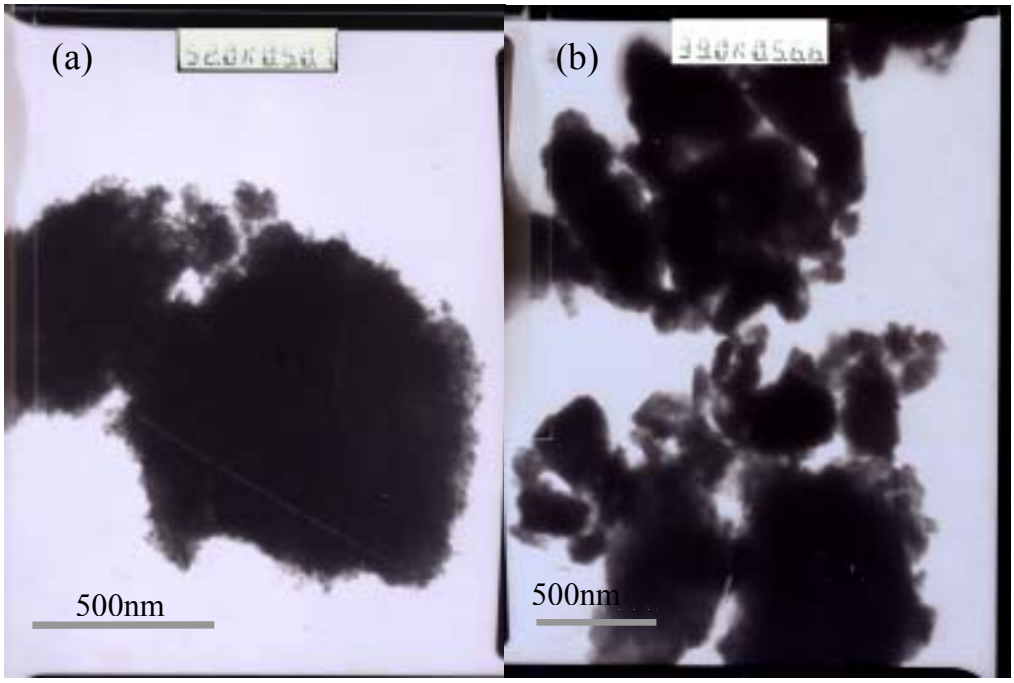

Figure 4.5. TEM images of the Ni-Ti composite xerogel catalysts cancined under different temperatures: (a) 613K for 10h and (b) 973K for 10h.

(Other preparation parameters: H=5.22; AC=0.10; Hydrolysis temperature:298K;

Drying temperature: 453K; Ni load: 10wt%)

whose respective atomic ratios over Ti are presented in Table 4.4. The XPS spectra of individual elements were shown in Figure 4.6. The catalyst calcined at 673K has the highest Ni/Ti ratio, 0.143, which is much larger than the bulk value, 0.042. The Ni/Ti ratios of the catalyst calcined at 473 and 973K are 0.079 and 0.059, respectively, which are close to the bulk value. The change of the surface Ni/Ti ratio may be indicative of the crystalline chages of the catalyst during the calcination. Results from XRD showed that the catalyst remains amorphous after calcination at 473K. The amorphous structutre helps to maintain the surface properites similar to the bulk. After calcination at 673K, only a distinctive brookite TiO_2 peak was observed from the XRD analysis and no significant Ni containg phase was observed. It may indicate that the crystallization of Ni occures from the surface of the catlyst first and that those in the bulk are still amorphous after calcination at 643K, leading to a higher Ni/Ti ratio. All components were totally crystallized after calcination at 973K and the surface ratio of Ni/Ti draws back close to the bulk level.

As indicated in the Ti2p pattern of the XPS spectra, peaks at the binding energy (BE) of around 463.5EV and 458.0EV, were typical of titanium (IV). The lower energy level of number 3 pattern at 457.9EV is attributed for the existence of TiO_3^{2-} [62], which is indicative of the existence of nickel titanate when calcination temperature was increased. This agrees with the XRD results. A third peak in pattern 1 was observed at 460.2EV, which is the attribution of titanium nitride [63]. The existence of titanium nitride was not detected in catalyst by X-ray analysis which may be due to its small amount.

Table 4.4. XPS Analysis of the Ni-Ti composite xerogel catalysts treated under different conditions

Calcination temperature (K)	Atomic Ratio Ni/Ti	Atomic Ratio C/Ti	Atomic Ratio N/Ti	Atomic Ratio O/(Ti+Ni)	Theoretical Ratio Ni/Ti
473	0.079	2.52	0.129	2.50	0.042
673	0.143	0.61	0.039	2.25	0.042
973	0.059	0.57	0.032	2.14	0.042

(Other preparation parameters: H=5.22; AC=0.10; Hydrolysis temperature:298K; Drying temperature: 453K; Ni load: 4wt%)

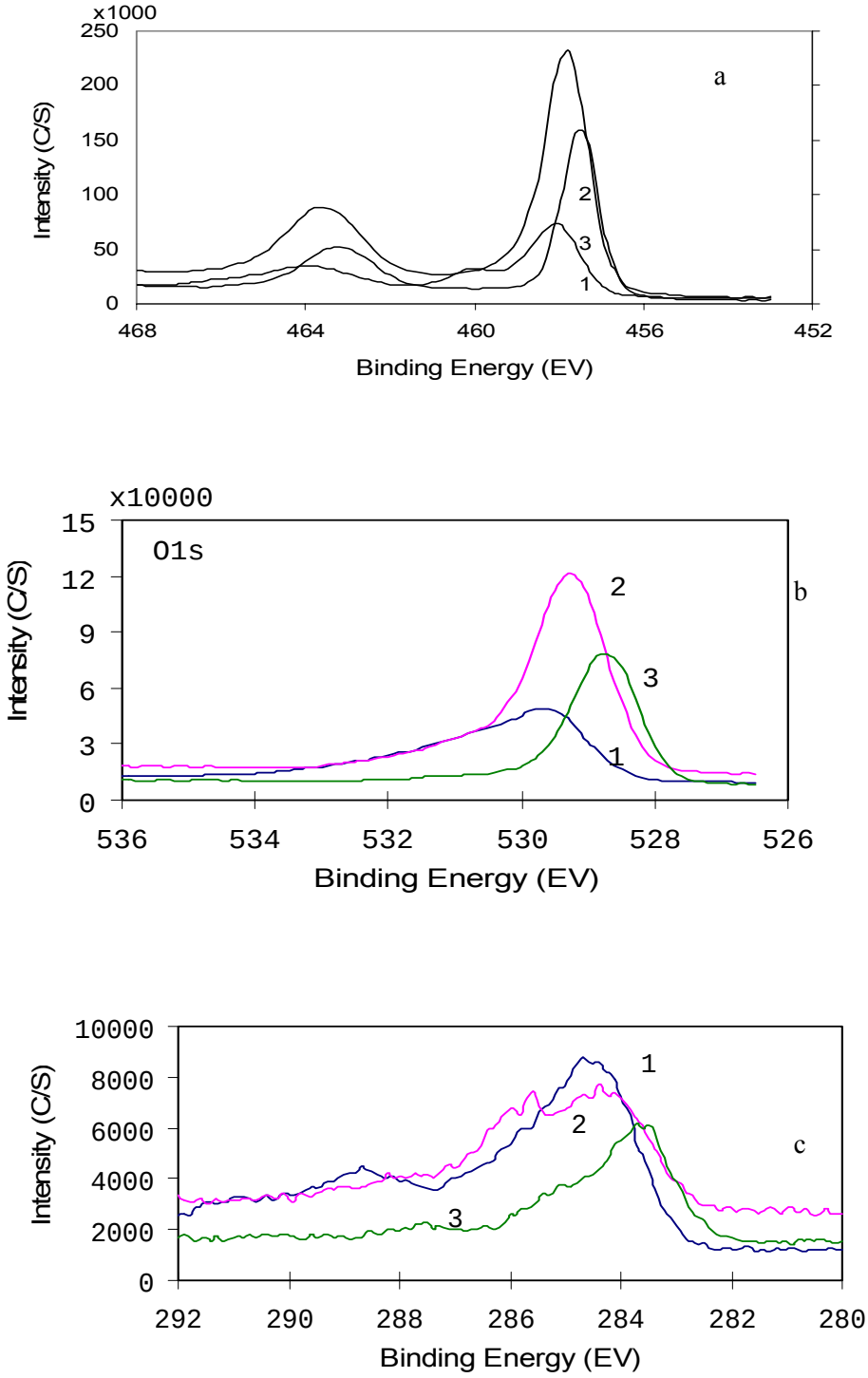

Figure 4.6. XPS analysis (a) Ti2p, (b) C1s, and (c) O1s of Ni-Ti xerogel catalysts treated under different conditions: (1): 473K for 10h; (2): at 673K for 10h; (3): at 973K for 10h. (Other preparation parameters are as the same as shown in Table 4.4)

Further examinations of C1s (c) and O1s (d) spectra indicate that multiple C and O species were present on the surface of catalysts after calcination at 473 and 673K (pattern 1&2). The C1s peak at the BE of 288.6EV indicates the existence of organic carbons. Since sample 1 and 2 were calcined at 473 and 673K, at which the calcination temperature was not high enough to decompose hydrocarbons, the shoulders in C1s and O1s of pattern 1 and 2, at 286.4EV and 531.1EV are indicative of complex species present on the surface. The symertic C1s and O1s peaks of the catalyst calcination after 973K indicate the simplicity of C and O species present on the surface, attributed to carbon in TiO_2 environment and oxygen in TiO_2 crystalline structure [64], respectively.

The atomic ratio of O/(Ni+Ti), ranging from 2.14 to 2.5, in disagreement with the nominal atomic composition of nickel titanium oxide, between 1.5 and 2, is indictive of excessive amount of O_2 present that could be attributed to the presence of OH groups on the surface. It is known that hydroxyl groups, such as Ti-OH, remain in the sol-gel prepared materials and promote the osteointegration process [65]. The decrease of the O/(Ni+Ti) as the calcination temperature increases is due to the "drying" effect which expels the –OH from the surface of the catalyst.

The surface property change can also be reflected by the SEM images shown in Figure 4.7. The catalyst calcined at 473K has shown bigger and even dispersed particles due to its amorphous structure. A large amount of small particles can be seen as calcination temperature increased to 773K due to the formation of small crystallites. As calcination temperature increased to 973K, the average particle is much larger than at 773K. It was

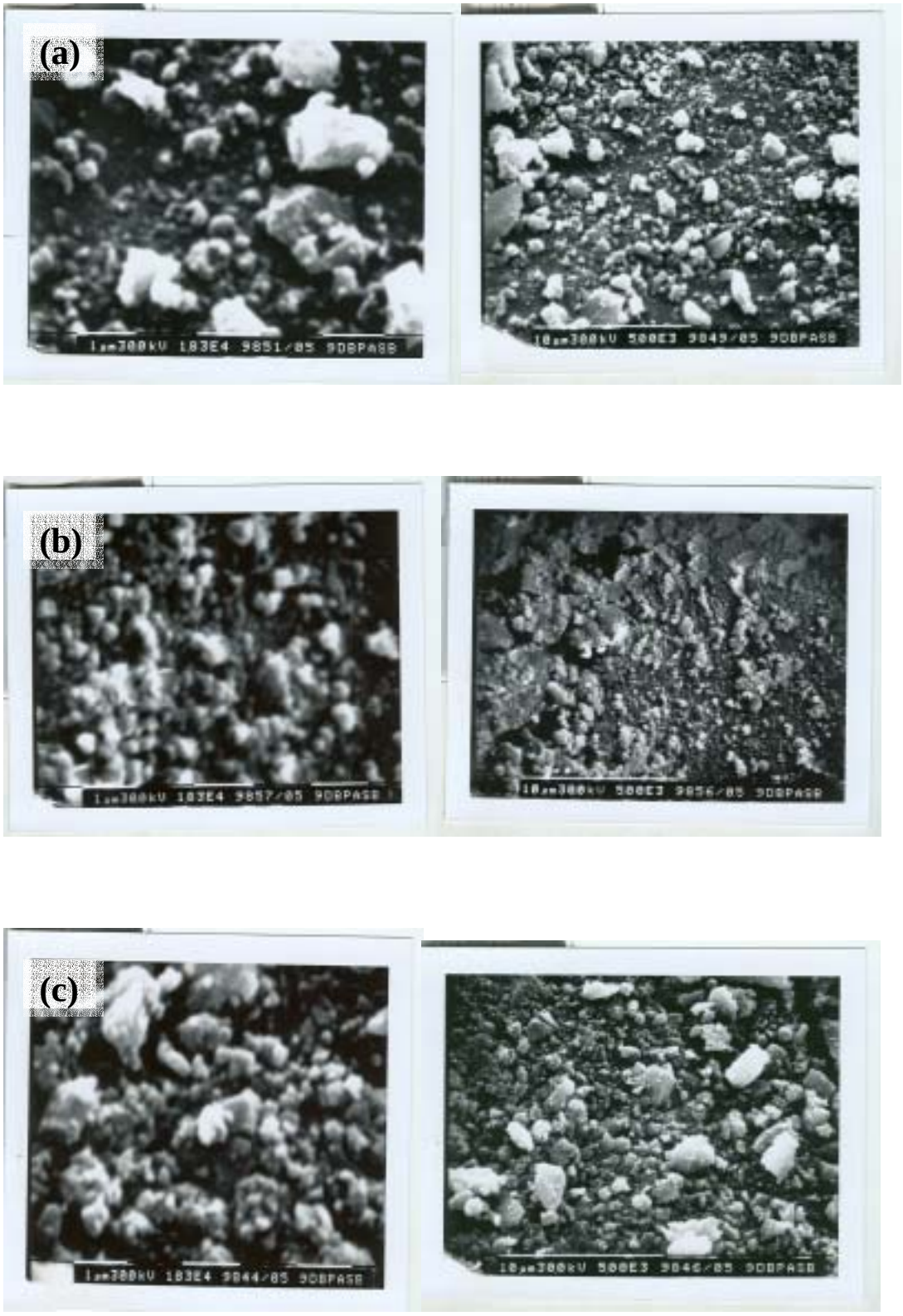

Figure 4.7. SEM images of Ni-Ti xerogel catalysts calcined at (a) 473K for 10h, (b) 773K for 10h and (c) 973K for 10h.

resulted by the aggregation of small particles due to the high temperature calcination. All these observations are in agreement with N_2 adsorption and XRD results. It was noticed that some sooth like material appears after the catalyst calcined at 773K. It doesn't attribute to carbon since XPS shows that most carbon has been removed at this point. XRD indicates that crystallization has developed and it has a significant smaller particle size comparing to catalyst calcined at 973K. It is reasonable to conclude that those fine powder like particles are the crystallized titania and nickel titanate.

4.2 Catalyst Evaluation

4.2.1 Thermodynamic Calculations of the Reactions

The equilibrium conversions of the four possible reactions, DRM, RWGS, CH_4 decomposition and CO disproportionation versus temperature are shown in Figure 4.8. Conclusions drawn from these calculations suggest that operation at high temperature, ~1100K, and with CO_2/CH_4 ratios far above unity can avoid regions where there is a thermodynamic potential for carbon formation; however, these conditions are not preferable from the industrial standpoint where lower operation temperature and CO_2/CH_4 ratio close to unity are expected. In addition, catalyst would sinter to deactivate itself if the reaction was operated over 1100K. In this thesis work, the catalyst evaluation process was operated at 973K, at which the equilibrium conversion of DRM is 80%.

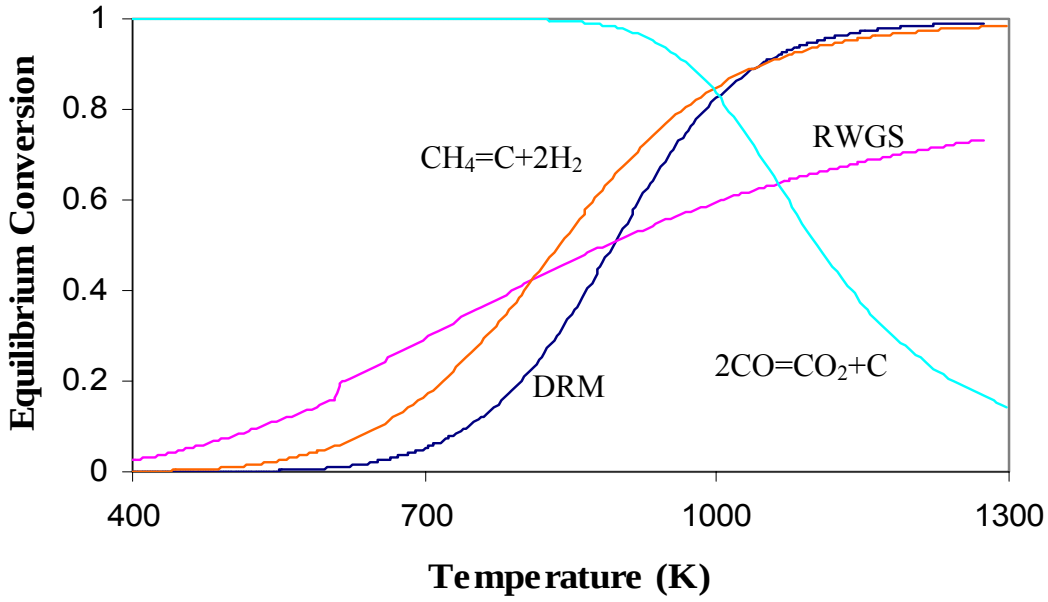

Figure 4.8. Thermodynamic calculations of four main reactions during the DRM. Reaction condition: P=100KPa, CH_4:CO_2=1:1.

4.2.2 Effect of Reduction Temperature on Catalyst Reactivity

It is believed that reduced Ni on catalyst surface is the active site for DRM. Thus the catalyst was reduced in the gas mixture of H_2 and N_2 (H2/N2=30/60 SCCM/min) before the reaction was carried out. To understand the catalyst reduction behaviour, the TPR analysis was conducted. As indicated in Figure 4.9, Ni in the sol-gel made catalyst requires higher temperature to get reduced than pure NiO. The difference is around 300K. In addition, not only the reduction peak of $NiTiO_3$ (at around 973K) was observed, but also the reduction of TiO_2 is present at around 1110K. The reduction of TiO_2 may have adverse impact on catalyst reactivity [35] while reduction at higher temperature gives more complete Ni reduction which favours the reaction. Therefore, it is meaningful to investigate the effect of reduction temperature on the reactivity of the catalyst.

Figure 4.10 indicates that the catalyst activity, with respect to the reaction rate of CH_4 and CO_2 (μmol/s/g-cat), increased as the reduction temperature was raised up from 823K to 973K. However, further increase in the reduction temperature to 1003K resulted in a dramatic decrease in the catalyst activity. The catalyst showed no activity at all after it had been reduced at 1023K and 1073K. When the reduction temperature was low, at 823K, as indicated by the TPR spectrum, the reduction level of the highly interacted catalyst was very low. The low reducibility of the $NiTiO_3$ at lower temperature directly contributes to its low activity. As the reduction temperature increases, the reduction level of the catalyst would increase. The XRD analysis in Figure 4.11 has proven that the catalyst reduced at 1023K for 4h obtained a 100% reduction

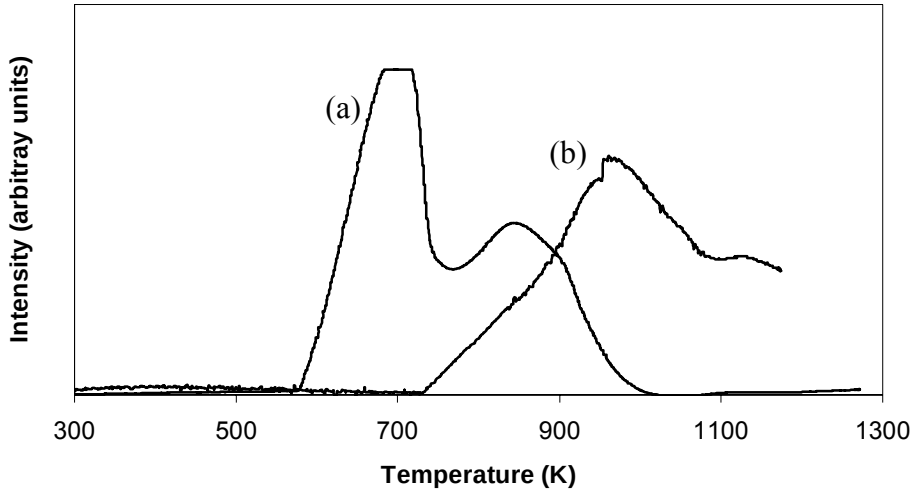

Figure 4.9. TPR analysis of (a) NiO and (b) 5 wt% Ni-Ti xerogel catalyst

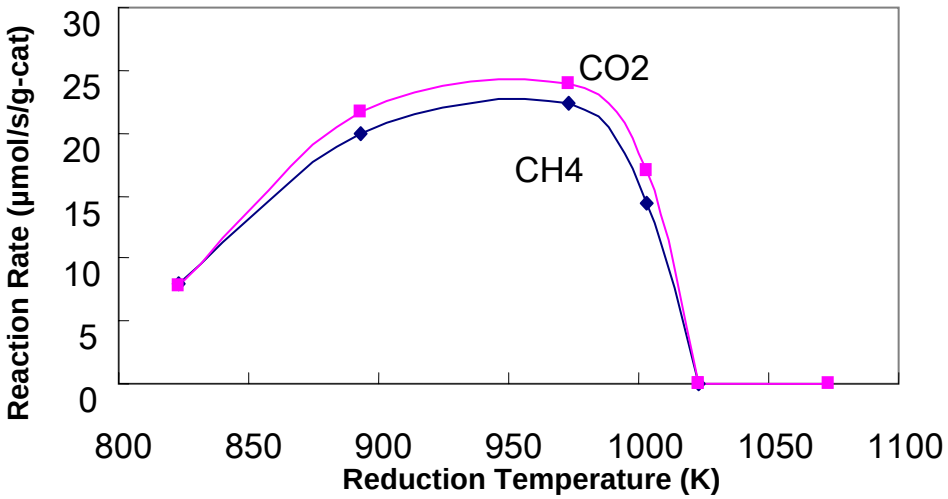

Figure 4.10. Effect of reduction temperature on the reactivity of catalysts. Reaction conditions: 5wt% Ni-Ti catalyst, P=1atm, T=973K, N_2:CH_4:CO_2=1.8:1:1, WHSV=10,000 SCCM/h/g-cat

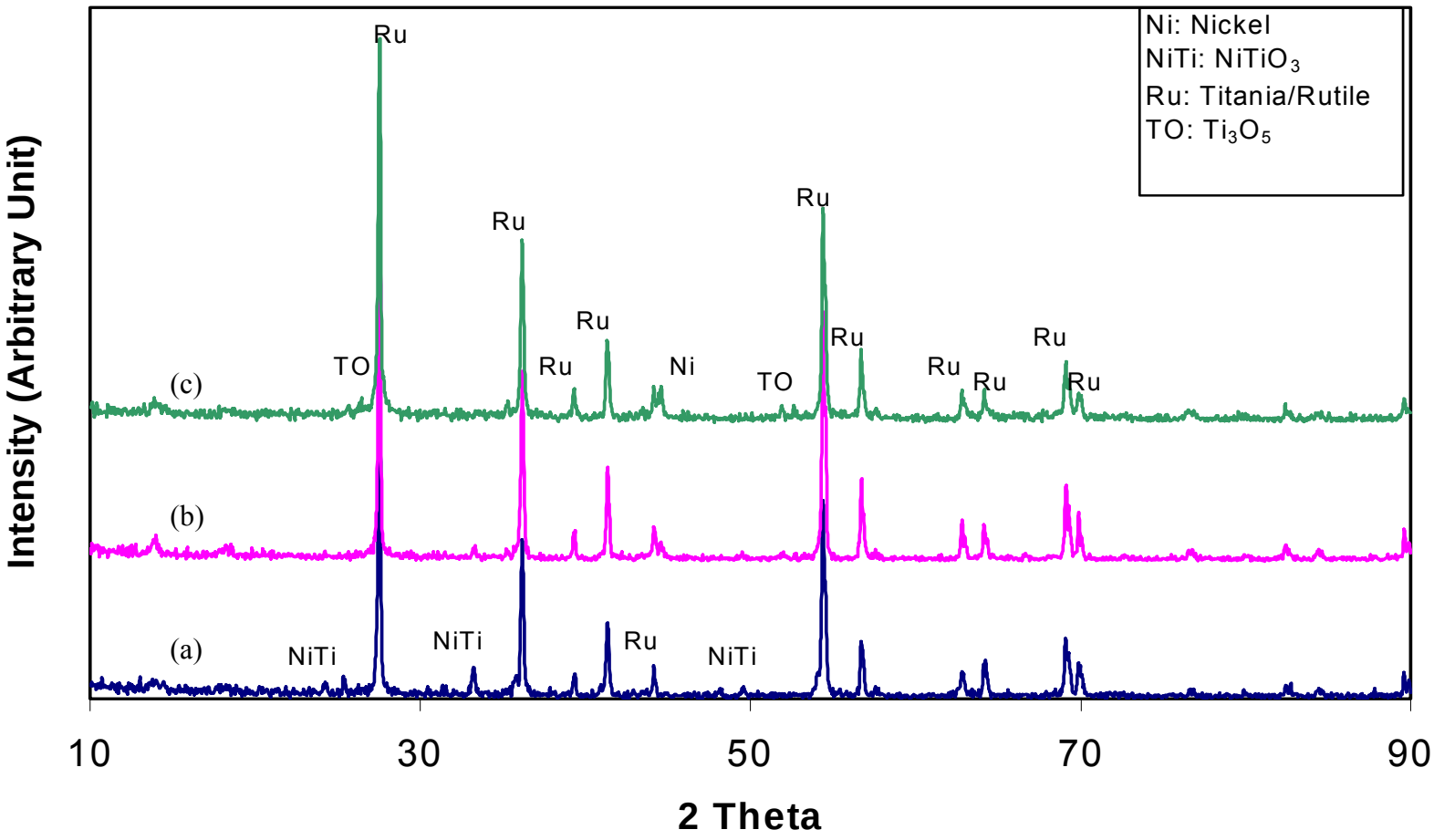

Figure 4.11. XRD analysis of 5wt% Ni-Ti xerogel catalysts (a) unreduced, (b) reduced at 973K for 4h, and (c) reduced at 1023K for 4h.

since no $NiTiO_3$ phase was observed but there was still some $NiTiO_3$ remaining unreduced after 4h at 973K. The higher reducibility indicates more active sites created. Thus, it can be theoretically said that the activity of the catalyst should increase with the reduction temperature. The XRD analysis of the catalyst reduced at 973K for 4h, pattern (b), shows very weak peaks appearing at the 2θ of 51.95 and 52.8. Both of them are attributed to the presence of Ti_3O_5. To the catalyst which was reduced at 1023K for 4h, the Ti_3O_5 peaks became more intensive, indicating that more Ti_3O_5 had formed. It was reported that TiO_2 can be reduced to form an oxide of TiO_x, where x is between 0 and 2 [33]. For example, Bradford et al. [33] has identified Ti_4O_7, Ti_3O_5, and Ti_5O_7 from the supported Ni/TiO_2 catalyst after 1h in H_2 stream at 773K, and assumed that these species would migrate to the surface of catalyst to cover active sites, so as to deactivate the catalyst. Since the only difference observed from the XRD patterns between the catalyst reduced at 973K and the one reduced at 1023K is that the latter one has higher intensity, corresponding to higher amount of Ti_3O_5, it seems that the formation of this new species has something to do with the loss of activity of the catalyst when it was reduced at a temperature over 973K. However, further studies are required to clarify the mechanism of this deactivation.

The other result drawn from the TPR and XRD characterizations is that the interaction between Ni and Ti is very strong. Pattern (a) of the XRD analysis shows $NiTiO_3$ is the only Ni-containing compound existing in the catalyst and no NiO is present. The temperature required for the reduction of $NiTiO_3$ is 973K, compared to 683K for the pure NiO. The broadness of the $NiTiO_3$ is indicative of not only the strong interaction

between Ni and Ti, but also the broad spread of the particle size in the catalyst after calcination at 973K.

Figure 4.12 shows the effect of reduction temperature on the ratio of H_2 to CO in product stream. It has the similar trend as the catalyst activity. The ratio increased as the temperature was elevated from 823 to 973K and dropped as the temperature increased to 1003K. Obviously, no H_2/CO ratio was presented for the catalysts reduced at 1023 and 1073K since the reaction rate was approaching 0. As discussed in the literature review, the RWGS reaction consumes the produced H_2 resulting in a higher conversion of CO_2 than CH_4 and a ratio of H_2/CO less than unit. When the catalyst was reduced at 973K, the catalyst showed higher activity and thus, large amount of CO_2 has been consumed for the DRM. So the amount of CO_2 left for the RWGS reaction is limited. This leads to a higher H_2/CO ratio. However, when the catalyst was reduced at a lower or higher temperature than 973K, the net available active sites was reduced, resulting in a lower activity. Consequently, the amount of CO_2 participating in the DRM reaction was reduced. The relatively larger amount of CO_2 remaining would stoichiometrically lead the RWGS reaction to the right side and result in the lower H_2/CO ratio.

4.2.3 Effect of Reduction Time on Catalyst Reactivity

Since reduction temperature has shown significant impact on the activity of catalysts, it seems that the reduction time can also affect their activities. The activities of the 5wt% Ni-Ti catalyst reduced in H_2 stream for various length of time (at 973K for 2, 4, and 6 hours) are shown in Figure 4.13. The results suggest that the longer reduction time

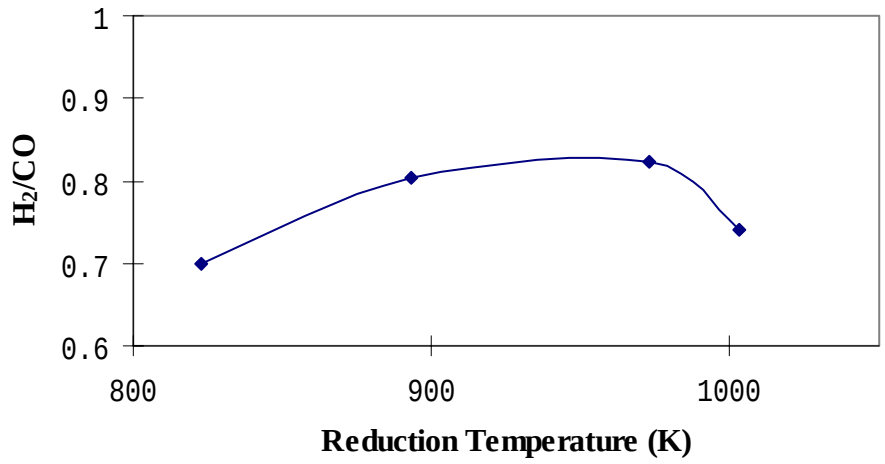

Figure 4.12. Ratio of H_2/CO in effluent over 5wt% Ni-Ti catalysts reduced at different temperatures. The reaction condition: P=1atm, T=973K, N_2:CH_4:CO_2=1.8:1:1, WHSV=10,000 SCCM/h/g-cat.

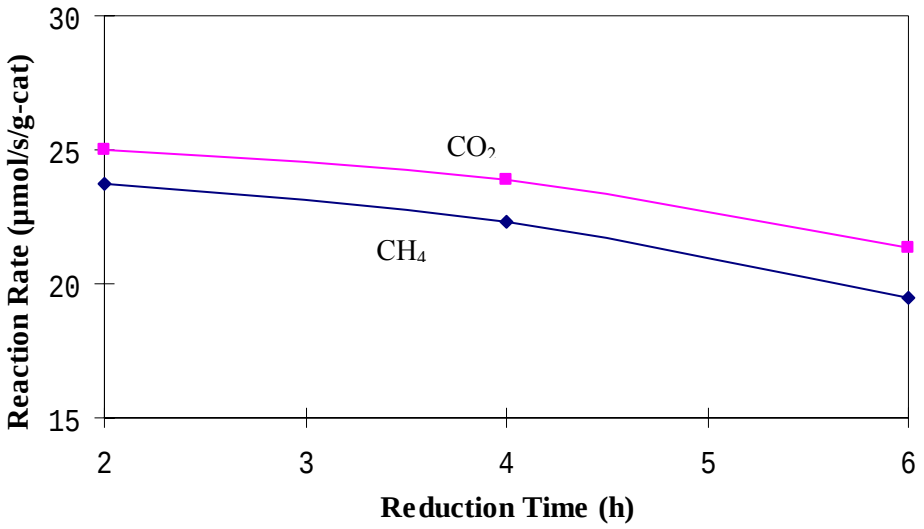

Figure 4.13. Effect of reduction time at 973K on the reactivity of catalysts. Reaction conditions: 5wt% Ni-Ti catalyst, P=1atm, T=973K, N_2:CH_4:CO_2=1.8:1:1, WHSV=10,000 SCCM/h/g-cat.

would lead to the lower activity of the catalyst. The catalyst reduced for 2h has shown relatively higher activity for both CH_4 and CO_2. The XRD analysis of the fresh catalyst and those reduced for different lengths of time is shown in Figure 4.14. It suggests that $NiTiO_3$ was reduced into elemental Ni, and the longer the reduction time, the higher the reduction level, possibly leading to a higher activity. However, the catalyst which had undergone longer reduction shows lower activity. Again, the observation of Ti_3O_5 formation on the catalyst that has been reduced for 6h may confirm that the appearance of Ti_3O_5 adversely impacts the catalyst activity. Since the reactant CH_4 and product H_2 supply a reduction environment for the catalyst, it raises a concern that Ti_3O_5 may form in the catalyst during DRM and thus lead to catalyst deactivation.

In summary, in order to obtain a high activity, the optimal reduction condition of the catalyst is 973K for 2h in H_2 and N_2 mixture. Thus, in the following experiments the catalysts were reduced under this condition.

4.2.4 Effect of Flow Rate of Feed Gas on Catalyst Reactivity

In order to find an area in which the reaction is controlled by the reaction rate of DRM, experiments of the effect of linear velocity of feed gas on the reaction rate with respect to CH_4 and CO_2 were conducted and the results are shown in Figure 4.15. Both CH_4 and CO_2 have a reaction rate of 25μmol/s/g-cat at a flow rate of 0.05m/s. The reaction rate of CH_4 and CO_2 increases to 55 and 75μmol/s/g-cat, respectively, when the linear velocity was increased from 0.05 to 0.25m/s. The reaction rate remains unchanged for CH_4 and keeps increasing for CO_2 when the linear velocity continues to increase. The stable stage of the reaction rate for CH_4 is indicative of a reaction control condition.

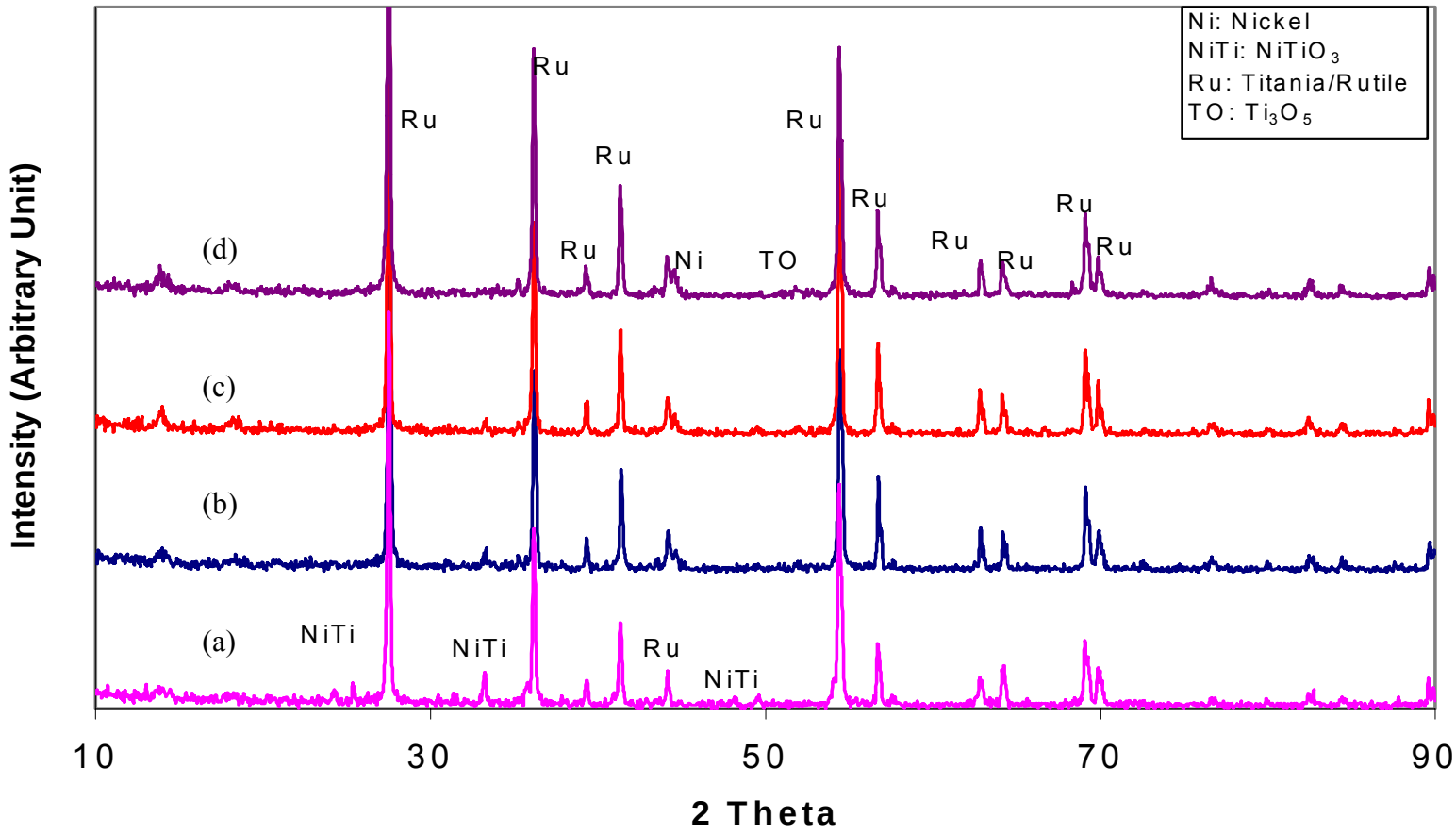

Figure 4.14. XRD analysis of 5wt% Ni-Ti xerogel catalysts (a) unreduced, (b) reduced at 973K for 2h, (c) reduced at 973K for 4h, and (d) reduced at 973K for 6h.

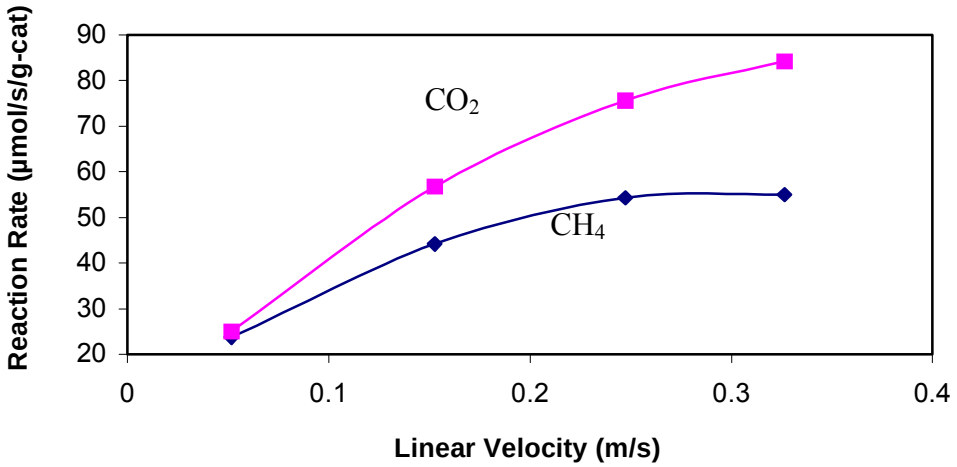

Figure 4.15. Effect of flow rate of feed gases on the reaction rate of catalysts reduced at 973K for 2h. Reaction conditions: 5wt% Ni-Ti catalyst, P=1atm, T=973K, N_2:CH_4:CO_2=1.8:1:1.

However the reaction rate of CO_2 continues to increase and no stable stage was observed. And it was also seen that the difference of reaction rate between CO_2 and CH_4 became larger with the increasing linear velocity. These phenomena are due to the existence of RWGS reaction. As indicated in Figure 4.16**,** a reverse trend was observed between the conversions of both CH_4 and CO_2 and linear velocity. When the linear velocity is 0.05m/s, the conversion of CH_4 and CO_2 is high, closing to the equilibrium conversion. As a result, the concentration of CO_2 in the stream is very low and, thermodynamically, it isn't preferential for the RWGS reaction. Reversely, when the linear velocity is 0.25m/s and the conversions of both CH_4 and CO_2 are low, the concentration of CO_2 in the stream is high. This is preferential for the RWGS reaction to consume the produced H_2. So the gap of the conversions between CH_4 and CO_2 becomes larger. As discussed previously, the reaction rate of DRM is the rate limit step when the linear velocity is over 0.25m/s. So the amount of CH_4 and CO_2 participating in the DRM reaction in the reaction control area is fixed. On the other word, when the linear velocity becomes even larger, 0.33m/s, the amount of CO_2 in the stream is more excessive, and, inevitably promotes the RWGS to the right side. So an unchanged reaction rate of CO_2 won't be reached until all produced H_2 is consumed by the RWGS if feed gas velocity keeps increasing.

In the following evaluation operations, in order to avoid the mass transfer control area, all runs were proceeded at a linear velocity of 0.25m/s, at which reaction rate of DRM is the rate limit step.

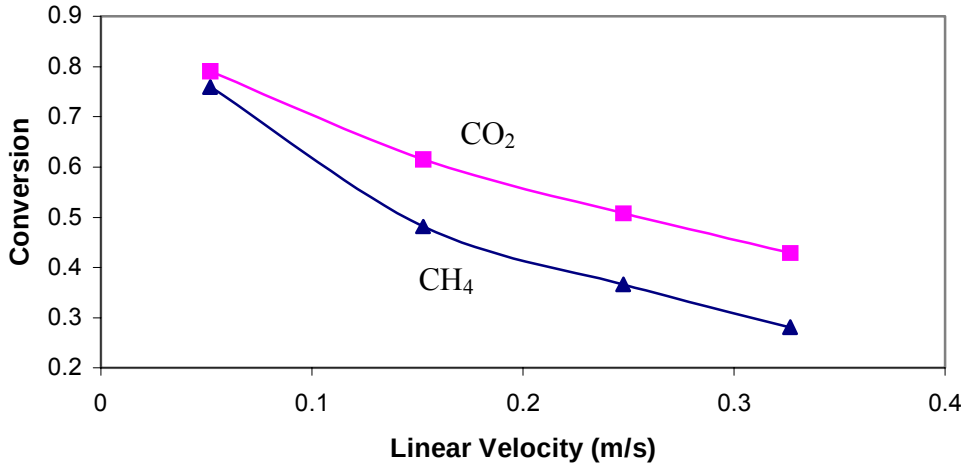

Figure 4.16. Effect of flow rate of feed gases on the conversion of catalysts reduced at 973K for 2h. Reaction conditions: 5wt% Ni-Ti catalyst, P=1atm, T=973K, N_2:CH_4:CO_2=1.8:1:1.

4.2.5 Effect of Nickel Load on Catalyst Reactivity

Catalysts with different Ni-loading were evaluated and the reaction rates of CH_4 and CO_2 are presented in Figure 4.17 and Figure 4.18, respectively. The catalysts were reduced at 973K for 2h. As discussed previously, due to the involvement of RWGS, the reaction rate of CO_2 is higher than CH_4. The reaction rate of both CH_4 and CO_2 is closely related with the Ni content and the higher the nickel content, the better the activity.

After 4h of time on stream, all evaluated catalysts have shown detectable deactivation. Especially during the first hour on stream, the 5wt% Ni-Ti catalysts lost 15% of its initial activity. Attempts have been made to understand the mechanism of catalyst deactivation during the use; but the results remain ambiguous. The XRD analysis of the 5wt% Ni-Ti catalyst before and after reaction is shown in Figure 4.19. By comparing pattern (b) to pattern (c), the unreduced $NiTiO_3$ peak disappeared and a couple of new peaks representing Ti_3O_5 appeared. It seems that the reaction mixture continues to reduce the catalyst during the reaction. And at the same time, reduction of TiO_2 to Ti_3O_5 was also occurring. As the concern brought previously, the formation of Ti_3O_5 may be responsible for the decrease of the catalyst activity. And this effect appears to be significant compared to continuing reduction that supposed to improve the activity. The deactivation rate of the catalyst became less after the first hour on stream as indicated in Figure 4.17. One possible reason for the decrease of deactivation rate is the slow down of the formation of Ti_3O_5. The other possible reason for this is that the catalysts need

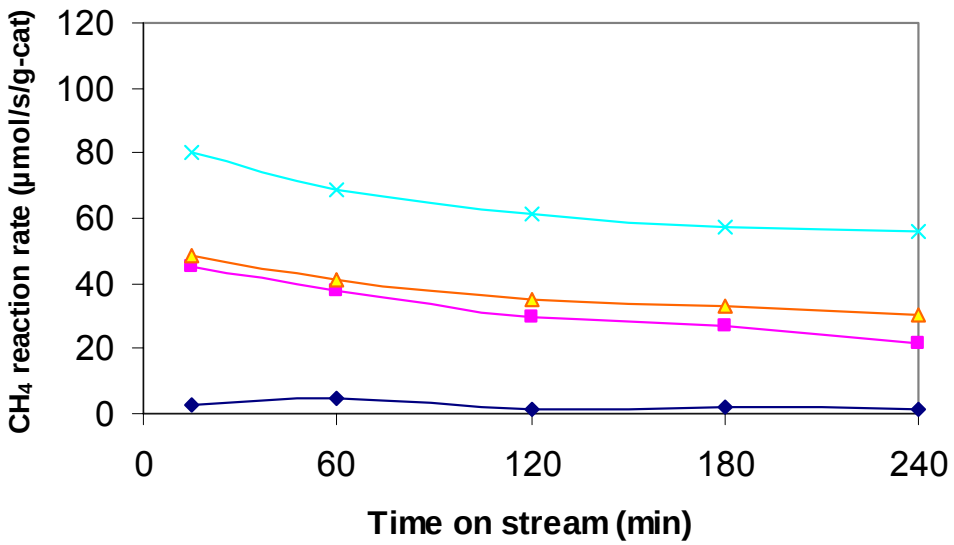

Figure 4.17. Effect of Ni load on the reaction rate with respect to CH_4, (×): 10wt%, (Δ): 5wt%, (■): 3wt%, and (♦): 1wt%. Reaction conditions: P=1atm, T=973K, N_2:CH_4:CO_2=1.8:1:1.

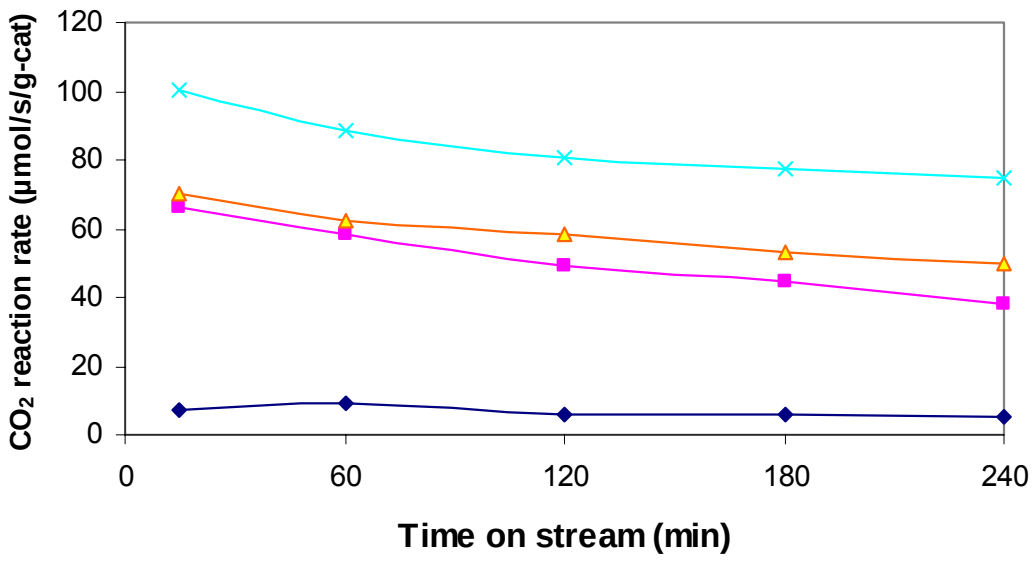

Figure 4.18. Effect of Ni load on the reaction rate with respect to CO_2, (×): 10wt%, (Δ): 5wt%, (■): 3wt%, and (♦): 1wt%. Reaction conditions: P=1atm, T=973K, N_2:CH_4:CO_2=1.8:1:1.

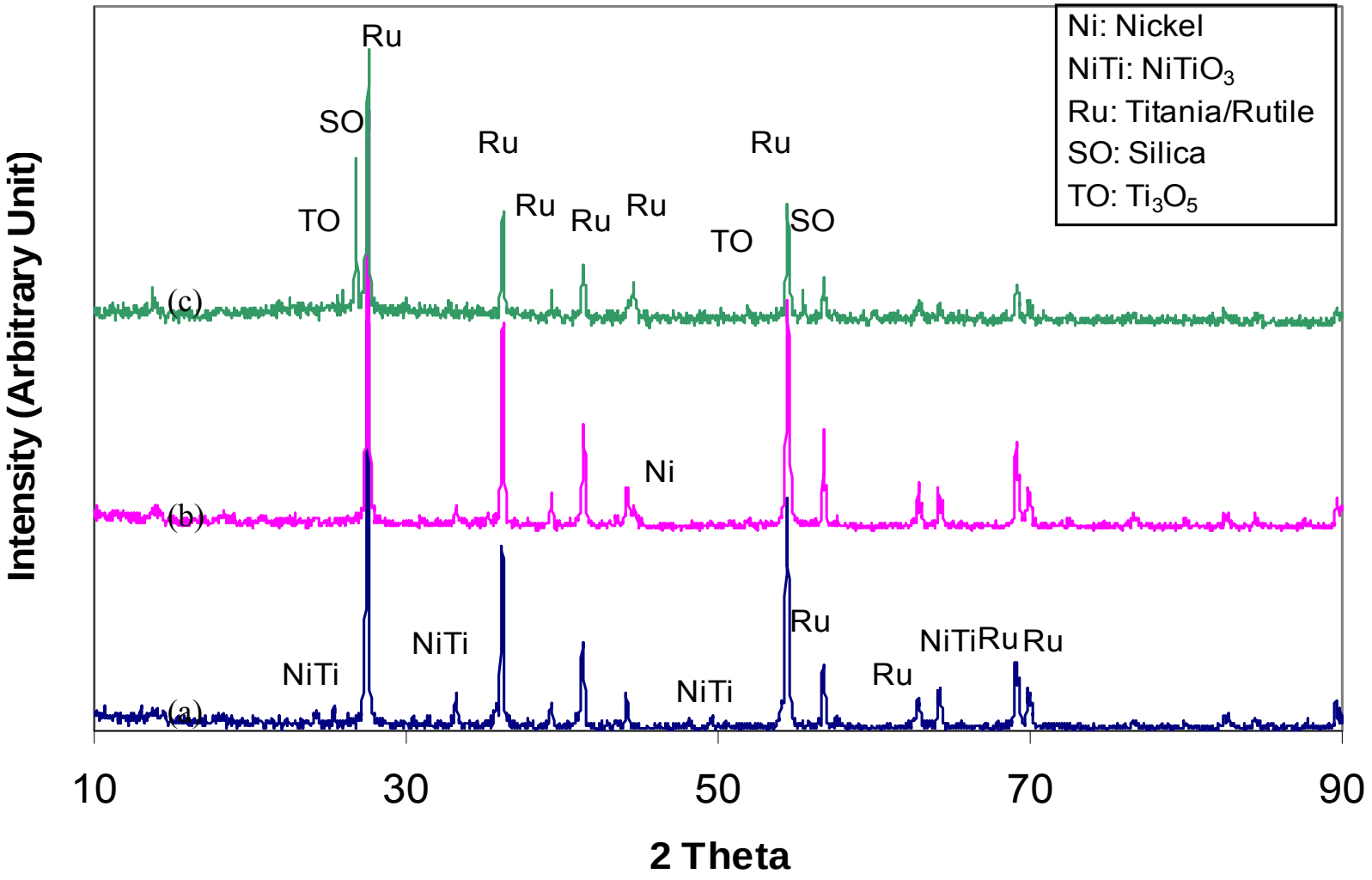

Figure 4.19. XRD analysis of 5wt% Ni-Ti xerogel catalyst (a) unreduced, (b) reduced at 973K for 2h, and (c) after 4h reaction.

time to get stabilized. Once they are stabilized, their activity may maintain constant. Longer experiment is required to prove this.

The other reason that may cause the deactivation of the catalysts is carbon deposition. A broad positive peak of pattern (c) starting from 773K to 923K in DTA analysis (Figure 4.20) was observed for the post-reaction catalyst. Compared to pattern (b) in the same figure for the catalyst before reaction, this peak corresponds an exothermic process that may be the combustion of carbon that has been deposited on the catalyst during the reaction. The TG results (Figure 4.21) support this view. To both the reduced and the post-reaction catalysts, the oxidation of elemental Ni into $NiTiO_3$ is the only source of weight increase. So the weight increase of the reduced catalyst from 773 to 110K was due to the oxidation of Ni into $NiTiO_3$ since the sample showed bright yellow after the TG/DTA analysis. From 773 to 923K, the slope of pattern (c) is smaller than that of pattern (b), indicating that the post-reaction catalyst gained less weight in this section. The post-reaction catalyst should have gained more weight since the reaction environment continues reducing it. So the only cause for the mitigation of the weight gain during 773 to 923K is due to combustion of the deposited carbon on the post-reaction catalysts. The gap between the two patterns at the end, 4.1mg/g-cat, can be used to estimate the amount of carbon that has been burned, indicating the amount of carbon that was deposited on the catalyst during the reaction. The average carbon deposition rate is 1.02mg/h/g-cat during the 4h. We realize that errors exist when this estimation was made. For example, the compositions of the pre- and post-reaction catalysts are slightly different due to the carbon deposition itself, and it was assumed that the diluting material and catalyst were well mixed.

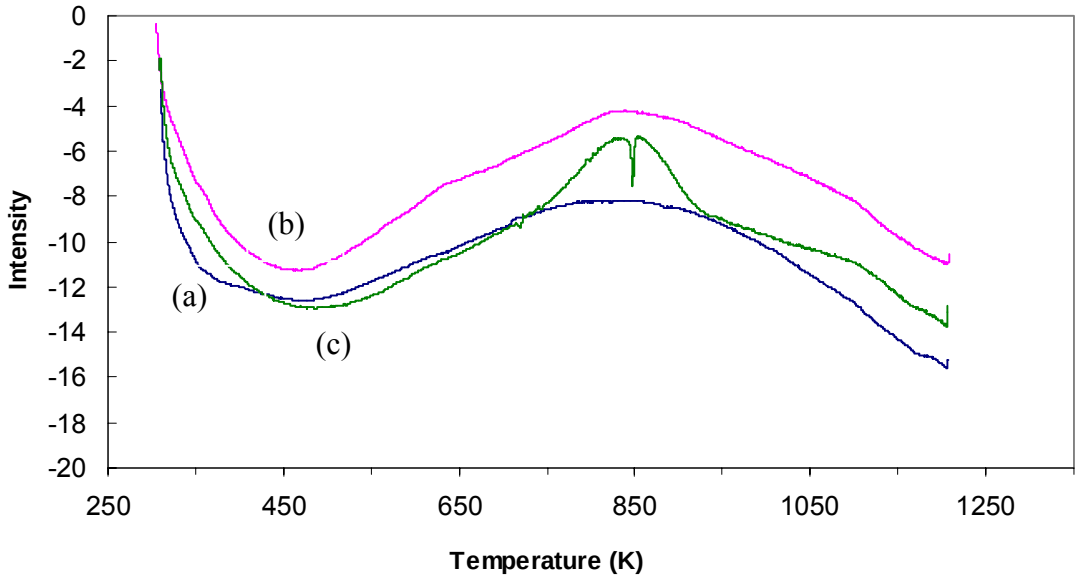

Figure 4.20. DTA analysis of 10wt% Ni-Ti xerogel catalyst (a) unreduced, (b) reduced at 973K for 2h, and (c) after 4h reaction.

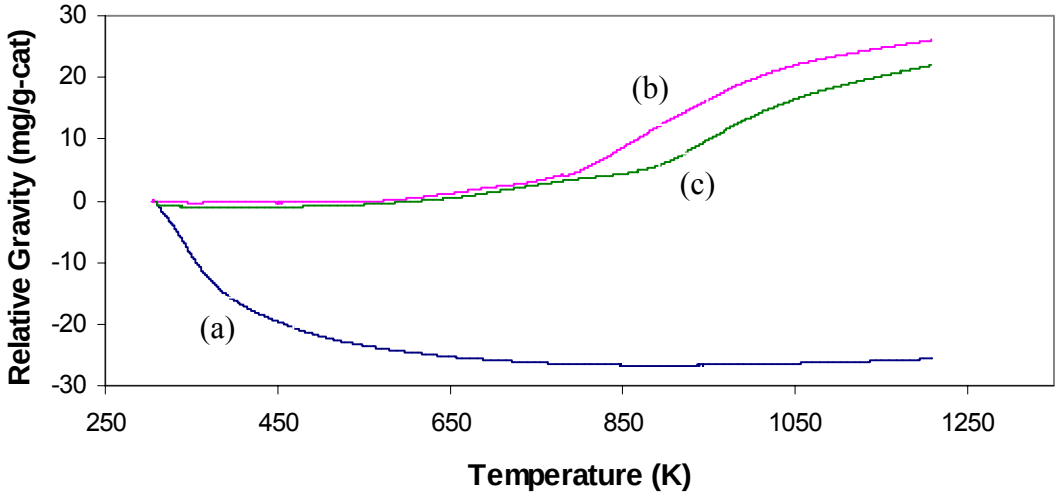

Figure 4.21. TG analysis of 10wt% Ni-Ti xerogel catalyst (a) unreduced, (b) reduced at 973K for 2h, and (c) after 4h reaction.

Quartz sands, which were used as the diluting material, could not be separated from the catalyst after reaction. The existence of quartz has been proven by the XRD analysis of the post-reaction catalyst sample which shows two silicon oxide peaks. It should be mentioned that the broad negative peak observed for all three samples from 300 to 500K are attributed to the evaporation of the moisture adsorbed on the samples when they were exposed to the atmosphere.

4.2.6 Effect of the Integration of Aluminium on Catalyst Reactivity

, Comparison shows that the Ni-Ti xerogel catalyst has lower reaction rate than the Ni catalysts supported by porous supports [33]. This may be due to the low surface area resulted from the high temperature calcinations which is inevitable for CO_2 reforming of CH_4. However, other measures that improve the catalyst surface area may increase the activity of the catalyst. In addition, since the interaction between nickel and titania is too strong resulting in poor reducibility, a third component which may help relieve the interaction between Ni and Ti so as to increase the reducibility of the catalyst is desired. Most importantly, a third component which could inhibit the reduction of TiO_2 into Ti_3O_5 would improve catalyst stability. Alumina has the nature of high surface area and developed porous structure. It was also reported that $NiAl_2O_4$ can form after calcination at 973K [6] which is easier to reduce than $NiTiO_3$. Therefore, the 5wt% Ni loading Ni-$Ti_{0.5}$-$Al_{0.5}$ catalyst was prepared using sol-gel method and evaluated under the same condition. The reaction activity is presented in Figure 4.22. Comparison with Figure 4.17 and 4.18 shows that the reaction rate is more than doubled as that of the 5wt% Ni-Ti catalyst. This is indicative that more active sites are available on the Ni-Ti-Al

catalyst than on the Ni-Ti catalyst. The surface area of this catalyst was not measured due to the failure of the BET apparatus. But from the physical observation, the

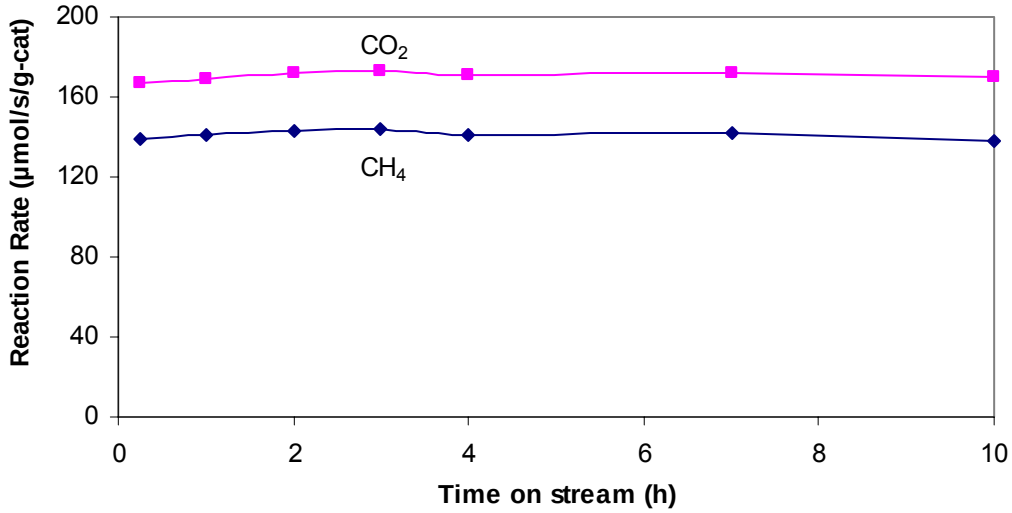

Figure 4.22. Reaction performance of 5wt% Ni-Ti-Al catalyst over DRM at the condition: P=1atm, T=973K, N_2:CH_4:CO_2=1.8:1:1, WHSV=90,000 SCCM/h/g-cat.

aluminium integrated catalyst has a much larger volume per mass since the addition of aluminium can help build porous structures and increase surface area of catalyst. The porous structure and high surface area can facilitate the dispersion of Ni and create more active sites with small particle size. In addition, the Ni-Ti-Al catalyst is more stable than the Ni-Ti catalyst. There wasn't noticeable deactivation observed to the aluminium integrated catalyst after 10h of time on stream.

The XRD analyses of the fresh, reduced and post-reaction Ni-Ti-Al catalyst are presented in Figure 4.23. There is still no pure NiO in the catalyst. Only small amount of $NiTiO_3$ was observed. Most Ni was present as the format of $NiAl_2O_4$. The Ni-Ti-Al catalyst was easier to reduce than the Ni-Ti catalyst since no nickel containing oxide was observed after the same reduction procedure. The high reducibility generated more active sites, attributing to its higher activity. Different to the Ni-Ti catalyst, no Ti_3O_5 observed after 2h reduction, and even after 10h reaction, further confirms the role of Ti_3O_5 that plays in catalyst deactivation. In other words, the addition of aluminium is able to inhibit the reduction of TiO_2. This may be the main reason that the Ni-Ti-Al catalyst can maintain higher activity and longer stability than the Ni-Ti catalyst. By comparing the XRD results of Ni-Ti catalyst and Ni-Ti-Al catalyst, all patterns in Figure 4.23 have shown broader peak wideness than those in Figure 4.19. The wider peaks suggest smaller particle size. As elaborated in the literature research, the smaller particles are preferential for the DRM rather than other side reactions [1]. As a result, the selectivity of H_2 and CO reaches as high as 0.83 and 1, respectively (Figure 4.24). The selectivity of CO above 1 in this figure may be due to the errors in GC calibration and analysis.

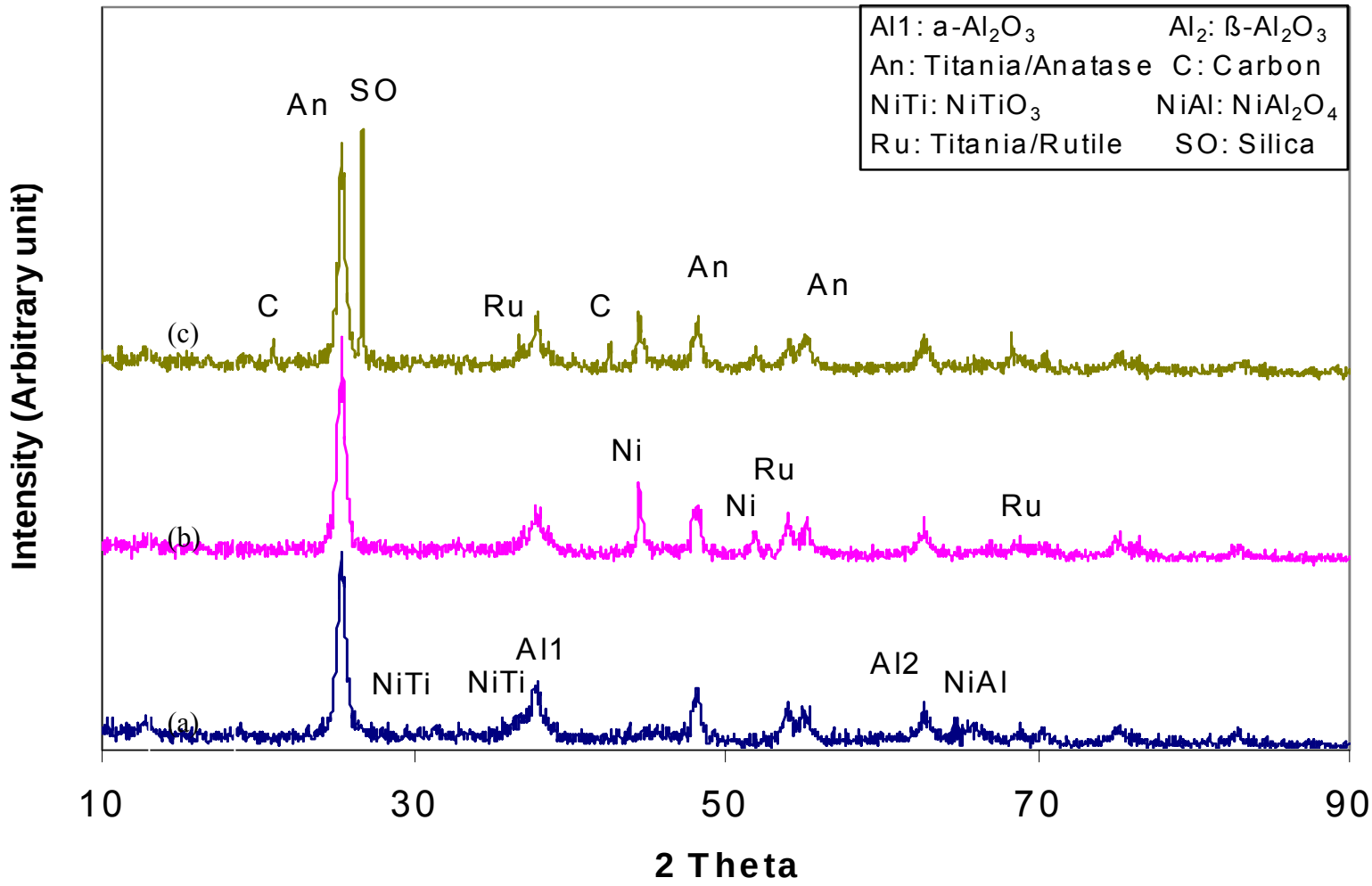

Figure 4.23. XRD analysis of 5wt% Ni-Ti-Al xerogel catalyst (a) unreduced, (b) reduced at 973K for 2h, and (c) after 10h reaction.

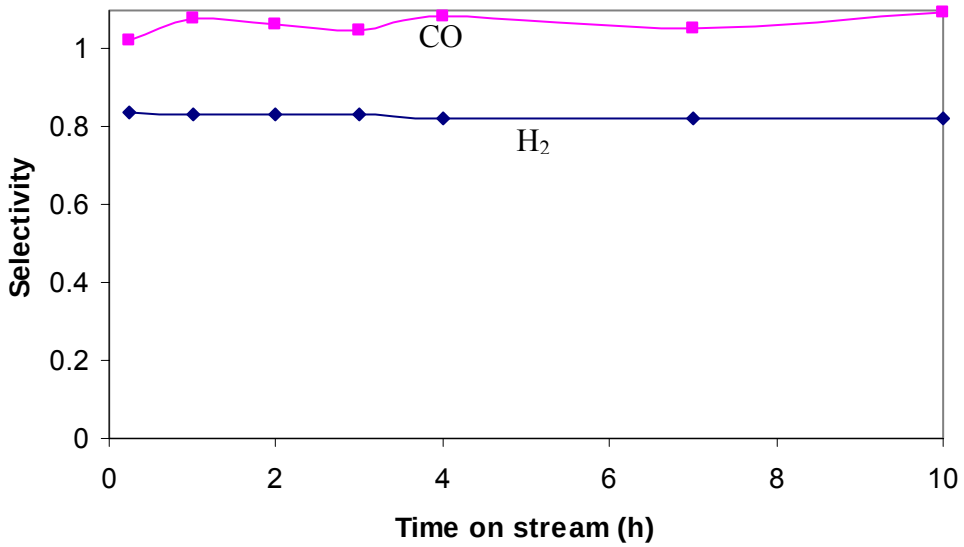

Figure 4.24. The ratio of H_2 to CO in effluent over 5wt% Ni-Ti-Al catalyst at the reaction condition: P=1atm, T=973K, N_2:CH_4:CO_2=1.8:1:1, WHSV=90,000 SCCM/h/g-cat.

As a consequence of the high reducibility, the reverse path of Ni reduction, presented in the DTA (Figure 4.25) and TG (Figure 4.26), is also easier. By comparing the TG/DTA analysis of Ni-Ti-Al catalyst to the pattern of Ni-Ti catalyst (Figure 4.20 and Figure 4.21), the oxidation of elemental Ni into $NiAl_2O_4$ occurred at temperature 500 to 750K, lower than the temperature 800 to 1050K for Ni-Ti catalyst to oxide Ni into $NiTiO_3$. It suggests that $NiAl_2O_4$ requires lower activation energy to reduce, corresponding to its higher reducibility than $NiTiO_3$. As shown in the XRD pattern, some carbon species formed on the Ni-Ti-Al catalyst after 10h of time on stream. The TG pattern of the post-reaction Ni-Ti-Al catalyst was observed a weight loss stage after the temperature at 720K. The weight loss is attributed to the removal of deposited carbon. Using the same estimation, the total carbon formed for a gram of catalyst in 10h is 20.8mg, or 2.1mg-C/h/g-cat in average, which is faster than the Ni-Ti catalyst. By comparing with the reported alumina supported 5wt% nickel catalyst at a rate of 11.3mg-C/h/g-cat [66] and co-precipitated 33wt% Ni-Al catalyst at a rate of 213 mg-C/h/g-cat [67], the sol-gel made Ni-Ti-Al catalyst has a much lower carbon deposition rate. The combination of Ni, Ti and Al in the catalyst using sol-gel method not only maintains the competitive activity but also improve the stability of the catalyst by suppressing the carbon deposition and preventing the reduction of TiO_2.

It is interesting to observe that titania presents as the crystallite of anatase in the Ni-Ti-Al catalyst after the calcination at 973K for 10h (Figure 4.23), but as rutile in the Ni-Ti catalyst shown in Figure 4.11. Rutile is a more stable and final phase of titania, and anatase transforms into rutile before 973K. As discussed in 4.1.3 Heat Effect on

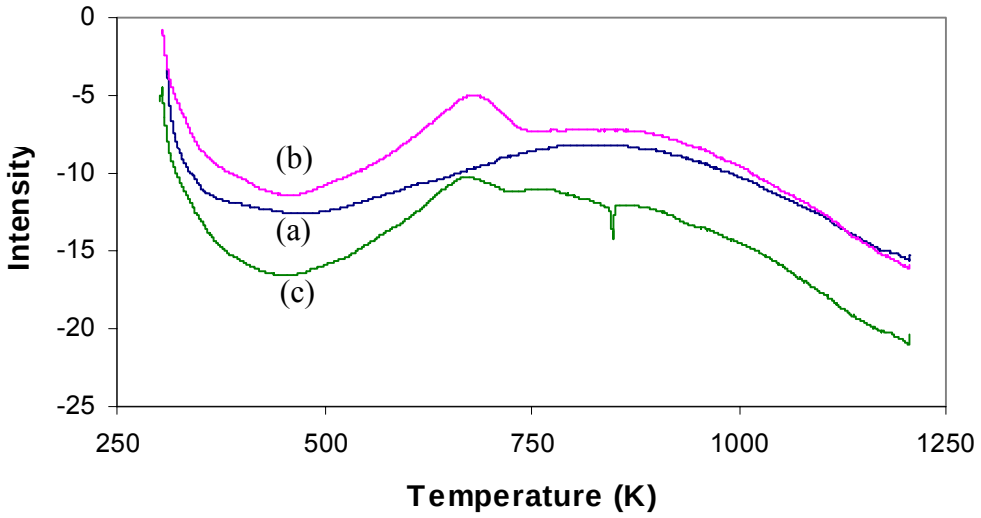

Figure 4.25. DTA analysis 5wt% Ni-Ti-Al catalyst (a) unreduced, (b) reduced at 973K for 2h, and (c) after 10h reaction.

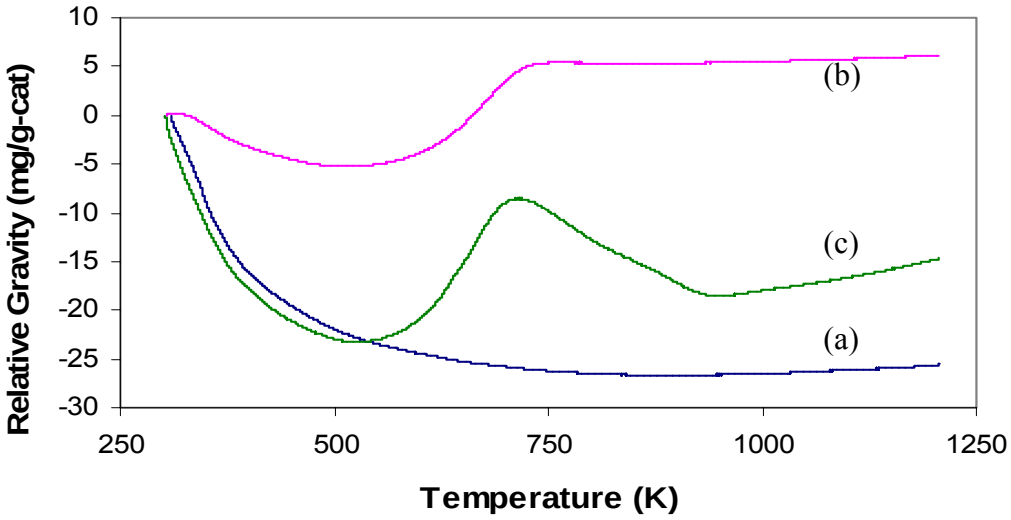

Figure 4.26. TG analysis of 5wt% Ni-Ti-Al catalyst (a) unreduced, (b) reduced at 973K for 2h, and (c) after 10h reaction.

Crystallite Structure, the extent of the coexistence of rutile and anatase may be due to the integration of aluminium. The existence of anatase, not rutile, may also contribute to the better performance of the catalyst.

It is worth noting that there is a sharp negative peak observed at the position of 850K in the DTA analysis for the post reaction Ni-Ti and Ni-Ti-Al catalysts, corresponding to an endothermic process. The possible chemical processes in the DTA analysis for the post reaction catalyst include the oxidation of elemental nickel, and the combustion of deposited elemental carbon. Both the combustion and the oxidation reactions are exothermic. So the possible contribution to this sharp negative peak may be due to desorption of a compound formed during the reaction.

CHAPTER 5

CONCLUSIONS AND RECOMMENDATIONS

The conclusions from this research can be drawn as follows:

1. Without rigorous care, such as supercritical CO_2 drying, inert gas protected calcination, and slow ramping of temperature in calcination process, sol-gel made Ni-Ti catalyst can reach as high as 426m^2/g BET surface area as long as the calcinations temperature maintains at no more than 473K.

2. The two important parameters in sol-gel process, the hydrolysis ratio, H, and the ratio of acid/alkoxide, AC, influence the resultant catalyst surface area and pore size. The optimum values of H and AC to obtain possible largest surface area have been determined in the particular range that this research chose.

3. Calcination temperature has a very significant impact on the surface area of the resultant catalyst. The Ni-Ti catalyst only have 2m^2/g surface area when made using sol-gel process described in this research followed by the calcination at 973K in air for 10h. Such calcination is inevitable for CO_2 reforming of CH_4 which would be carried out at a temperature close to 973K to obtain a reasonable conversion. Collapse of porous structure and crystallization during the high temperature calcinations lead to the surface area loss.

4. The Ni loading up to 10wt% in sol-gel made Ni-Ti xerogel catalysts show different properties than pure TiO_2. For example, the phase transformation temperatures, such as from amorphous to brookite and from brookite to anatase and rutile have been increased and anatase and rutile coexist even after being calcined at 973K for 10h. The formation of $NiTiO_3$ has been observed. It seems that no NiO exists in the catalysts.

5. The reduction temperature has strong effect on the Ni-Ti catalyst activity. The activity increases as the reduction temperature increases up to 973K. But further increasing the reduction temperature renders the drastic decrease in activity till the catalyst losses all the activity when it had been reduced at 1023K or higher. Longer reduction time than 2h also causes the activity to decrease. The formation of Ti_3O_5 during reduction may be one of the reasons that lead to this activity losses; but to clarify the mechanism needs further studies.

6. The reaction rate controlling regime is determined when the linear velocity is 0.25m/s or larger. At this regime, more Ni loading gives higher activity.

7. Carbon deposition is observed and activity decay is detected during the 4h of time on stream of the Ni-Ti catalyst.

8. The sol-gel made Ni-Ti-Al catalyst gives more than 2 times higher activity than the Ni-Ti catalyst and no noticeable deactivation is observed after 10h of time on stream. Carbon deposition is also found in the reaction over this catalyst.

Based on this research, further investigations should focus on the following respects:

1. Determining the optimum composition of Ni-Ti-Al sol-gel made catalyst, evaluating this catalyst in a longer time period, and studying the mechanism of the activity and stability improvement.

2. Further studying the mechanism of the effect of reduction temperature on reaction activity for Ni-Ti sol-gel catalyst.

3. Completing the standardization of the sol-gel process in preparation of Ni-based catalysts for the dry reforming of CH_4 reaction.

REFERENCE

1 M.C.J. Bradford, and M.A. Vannice, CO_2 Reforming of CH_4 *Catal. Rev.: Sci. Eng* **41 (1)** (1999), p.1.

2 "Carbon sequestration projects" DOE Fossile office Web Site. <http://www.fossil.energy.gov/fred/feprograms.jsp?prog=Carbon+Sequestration> 16 Dec 2004

3 "Carbon sequestration projects" DOE Fossile office Web Site. <http://www.fossil.energy.gov/fred/feprograms.jsp?prog=Carbon+Sequestration> 16 Dec 2004

4 Y. Soong, A.L. Goodman, J.R. McCarthy-Jones, J.P. Baltrus, *Energy Conversion and Management* **45 (11-12)** (2004), P.1845.

5 F. Fischer, and H. Tropsch, *Brennstoff Chem.* **3 (39)** (1928)

6 S. Tang, L. Ji, J. Lin, H.C. Zeng, k.L. Tan, and K. Li, CO_2 Reforming of methane to synthesis gas over Sol-gel made Ni/γ-Al_2O_3 catalysts from organometallic precursors *J. of Catal.* **194** (2000), p.424.

7 J.T. Richardson, M. Garrait, J.-K. Hung, Carbon dioxide reforming with Rh and Pt–Re catalysts dispersed on ceramic foam supports *Appl. Catal. A: General* **255** (2003), p.69.

8 R. Martínez, E. Romero, C. Guimon and R. Bilbao, CO_2 reforming of methane over coprecipitated Ni–Al catalysts modified with lanthanum *Appl. Catl. A: General* **274, (1-2)** (2004), p.139.

9 S-H, Lee, D.J., Suh, T-J Park, and K-L Kim, The effect of heat treatment conditions on the textural and catalytic properties of Nickel-titania Composite aerogel catalysts *Catal. Communi.* **3** (2002), p.441.

10 M. C. J., Bradford, and M. A., Vannice, CO_2 reforming of CH_4 over supported Pt catalysts *J. Catal.* **173** (1998), p.157.

11 Q.G. Yan, W.Z. Weng, H.L. Wan, H.Toghiani, R.K. Toghiani, and C.U. Pittman, Jr., Activation of methane to syngas over a Ni/TiO_2 catalyst *Appl. Catl. A: General* **239** (2003), p.43.

12 K. Tomishige, and K. Fujimoto, Ultra-stable Ni catalysts for methane reforming by carbon dioxide *Catalysis surveys from Japan* **2** (1998), p.3.

13 D.J. Suh, T.J. Park, Y.H. Yoon, and J.H. Kim, Nickel-alumina aerogel catalyst for carbon dioxide reforming of methane and the preparation method thereof, US patent, # *6-355-219,* (2002).

14 S. Wang, G.Q. Lu, Reforming of methane with carbon dioxide over Ni/Al_2O_3 catalysts: Effect of nickel precursor *Appl. Catl. A: General* **169** (1998), p.271.

15 O. Yamazaki, T. Nozaki, K. Omata, and K. Fujimoto, *Chem. Lett.*, **1953** (1992).

16 A. A. Lemonidou, I. A. Vasalos, Carbon dioxide reforming of methane over 5 wt.% Ni/CaO-Al_2O_3 catalyst *Appl. Catl. A: General* **228** (2002), p.227.

17 J. A. C. Dias, and J. M. Assaf, Influence of calcium content in Ni/CaO/γ -Al_2O_3 catalysts for CO_2-reforming of methane *Catal. Today* **85** (2003), p.59.

18 A. Takano, T. Tagawa, and S. Goto, *J. Chem. Eng. Japan* **27** (1994), p.727.

19 S.-B. Tang, F.-L. Qiu, and S.-J. Lu, Effect of supports on the carbon deposition of nickel catalysts for methane reforming with CO_2 *Catal. Today* **24** (1995), p.253.

20 Z. Chang, Q. Wu, J. Li, and Q. Zhu, Effects of promoters and preparation procedures on reforming of methane with carbon dioxide over Ni/Al_2O_3 catalyst *Catal. Today*, *30*, 147 (1996).

21 C. Batiot-Dupeyrat, G. Valderrama, A. Meneses, F. Martinez, J. Barrault, J.M. Tatibouët, Pulse study of CO_2 reforming of methane over $LaNiO_3$ *Appl. Catl. A: General* **248** (2003), p.143.

22 V. A. Tsipouriari, and X. E. Verykios, Kinetic study of the catalytic reforming of methane with carbon dioxide to synthesis gas over Ni/La_2O_3 catalyst *Catal. Today* **64** (2001), p.83.

23 M. C. J. Bradford, Ph.D. thesis, The Pennsylvania State University (1997)

24 S.-H Seok, S.H. Choi, E.D. Park, S.H. Han, and J.S Lee, Mn-promoted Ni/Al_2O_3 catalysts for stable carbon dioxide reforming of methane *J. Catal.* **209** (2002), p.6.

25 S.-H Seok, S.H. Han, J.S. Lee, The role of MnO in $Ni/MnO\text{-}Al_2O_3$ catalysts for carbon dioxide reforming of methane *Appl. Catl. A: General* **215** (2001), p.31.

26 R. Moene, Ph.D dissertation, Delft University of Technology (1995).

27 J. R. Rostrup-Nielsen and J.-H. Bak Hansen, CO_2-Reforming of Methane over Transition Metals *J. Catal.*, **144** (1993), p.38.

28 V. C. H. Kroll, H. M. Swaan, and C. Mirodatos, Methane reforming reaction with carbon dioxide over Ni/SiO_2 catalyst: I. deactivation studies *J. Catal.* **161** (1996), p.409.

29 V. R. Choudhary, B. S. Uphade, and A. S. Mamman, *Catal. Lett.* **32** (1995), P.387.

30 E. Ruckenstein, and Y. H. Hu, Carbon dioxide reforming of methane over nickel/alkaline earth metal oxide catalysts *Appl. Catal. A. General* **133** (1995), p.149.

31 Q. Jing, H. Lou, J. Fei, Z. Hou, X. Zheng, Syngas production from reforming of methane with CO2 and O2 over Ni/SrO–SiO2 catalysts in a fluidized bed reactor International *J. of Hydrogen Energy* **29** (2004), p.1245.

32 M. C. J. Bradford and M. A. Vannice, Catalytic reforming of methane with carbon dioxide over nickel catalysts II. Reaction kinetics *Appl. Catal. A.: General* **142** (1996), p.97.

33 M. C. J. Bradford and M. A. Vannice, Catalytic reforming of methane with carbon dioxide over nickel catalysts I. Catalyst characterization and activity *Appl. Catal. A.: General* **142** (1996), p.73.

34 T. Osaki, H. Masuda, and T. Mori, *Catal. Lett.* **29** (1994), p.33.

35 H-S Roh, H.S. Potdar, K-W Jun, Carbon dioxide reforming of methane over co-precipitated Ni–CeO_2, Ni–ZrO_2 and Ni–Ce–ZrO_2 catalysts *Catal. Today* **93-95** (2004), p.39.

36 J. A. Montoya, E. Romero-Pascual, C. Gimon, P. Del Angel and A. Monzón, Methane reforming with CO_2 over Ni/ZrO_2–CeO_2 catalysts prepared by sol–gel *Catal. Today* **63** (2000), p.71.

37 H-S Roh, H.S. Potdar, K-W Jun, J-W Kim, and Y-S Oh, Carbon dioxide reforming of methane over Ni incorporated into Ce–ZrO_2 catalysts *Appl. Catal. A: General* **276** (2004), p.231.

38 J.-S. Chang, S.-E. Park, and H. Chon, Catalytic activity and coke resistance in the carbon dioxide reforming of methane to synthesis gas over zeolite-supported Ni catalysts *Appl. Catal. A: General* **145** (1996), p.111.

39 B. Ølgaard Nielsen, A. C. Luntz, P. M. Holmblad, and I. Chorkendorff, *Catal. Lett.* **32** (1995), p.15.

40 D. C. Seets, M. C. Wheeler, and C. B. Mullins, *Chem. Phys. Lett.* **266** (1997), p.431.

41 E. O. F. Zdansky, A. Nilsson, and N. Mårtensson, CO-induced reversible surface to bulk transformation of carbidic carbon on Ni(100) *Surf. Sci.* **310** (1994), L583.

42 V. V. Chesnokov, V. I. Zaikovskii, R. A. Buyanov, V. V. Molchanov, and L. M. Plyasova, Morphology of carbon from methane on nickel-containing catalysts *Catal. Today* **24** (1995), p.265.

43 T. Horiuchi, K. Sakuma, T. Fukui, Y. Kubo, T. Osaki, and T. Mori, Suppression of carbon deposition in the CO_2-reforming of CH_4 by adding basic metal oxides to a Ni/Al_2O_3 catalyst *Appl. Catal. A: General* **144** (1996), p.111.

44 Z. L. Zhang, and X. E. Verykios, Carbon dioxide reforming of methane to synthesis gas over supported Ni catalysts *Catal. Today* **21** (1994), p.589.

45 H. M. Swaan, V. C. H. Kroll, G. A. Martin, and C. Mirodatos, Deactivation of supported nickel catalysts during the reforming of methane by carbon dioxide *Catal. Today* **21** (1994), p.571

46 V. A. Tsipopuriari, A. M. Efstathiou, Z. L. Zhang, and X. E. Verykios, Morphology of carbon from methane on nickel-containing catalysts *Catal. Today* **21** (1994), p.579

47 Y.-G. Chen, and J. Ren, *Catal. Lett.* **29** (1994), p.39.

48 Y. H. Yu, and E. Ruckenstein, Temperature-Programmed desorption of CO adsorbed on NiO/MgO *J. Catal.* **163** (1996), p.306.

49 O.-S. Joo, and K.-D. Jung, CH_4 dry reforming on alumina-supported nickel catalyst *Bull. Korean Chem. Soc.* **23, (8)** (2002), P.1149.

50 J. R. Rostrup-Nielsen, *Stud. Surf. Sci. Catal.* **68** (1991), p.85.

51 L. Mleczko, S. Malcus, and T. Wurzel, Catalytic reformer-combustor: a novel reactor concept for synthesis gas production. *Ind. Eng., Chem. Res.* **36** (1997), p.4459.

52 T. Wurzel, S. Malcus, L. Mleczko, Reaction engineering investigations of CO_2 reforming in a fluidized-bed reactor *Chem. Eng. Sci.* **55** (2000), p.3955.

53 A.I. Tsyganok, K. Suzuki, S. Hamakawa, K. Takehira, and T. Hayakawa, Mg-Al layerer double hydroxide intercalated with [Ni(edta)]2- chelate as a precursor for an efficient catalyst of methane reforming with carbon dioxide *Catalysis Letters* **77** (2001), p.1.

54 W-S Dong, H-S Roh, K-W Jun, S-E Park, and Y-S Oh, Methane reforming over Ni/Ce-ZrO_2 catalysts: effect of nickel content *Applied catal. A: General* **226** (2002), p.63.

55 K. Hwang, H.Y. Zhu, and G.Q.Lu, New nickel catalysts supported on highly porous alumina intercalated laponite for methane reforming with CO_2 *Catal. Today* **68** (2001), p.183.

56 P. Zheng, H.Y. Zhu, and G.Q.Lu, Zr-Laponite pillared clay-based catalysts for methane reforming with carbon dioxide *Applied Catal. A: General* **242** (2003), p. 275.

57 G. Ertl, H. Knözinger, J. Weitkamp, in Preparation of Solid Catalysts (1999), P.95.

58 C.J., Brinker, G.W., Scherer, in Sol-Gel Science – the physics and chemistry of sol-gel processing *Academic press, INC* (1990)

59 M., Schneider, A., Baiker Review, Yitania-based aerogels *Catal. Today* **35** (1997), P.339.

60 D.J. Taylor, P.F. Fleig, R.A. Page, *Thin Solid Films* **408** (2002), p.104.

61 Y. Zhang, and A. Reller, *Chem. Commun* (2002), p.606.

62 M. Wakamatsu, N. Takeuchi, G.-C. Lai, *Yogio-kyokaishi* **95** (1987), p.1181.

63 B.J. Burrow, A.E. Morgan, R.C. Ellwanger, *J. vac. Sci. Technol.* **A4** (1986), p.2463.

64 V.I. Nefedov, D. Gati, B.F. Dzhurinskii, N.P. Sergushin, Y.V. Salyn, *Russian Journal of Inorganic Chemistry* **20** (1975), p.2307.

65 E. Milella, F. Cosentino, A. Licciulli, C. Massaro, *Biomaterials* **22** (2001), p1425.

66 T. Tanaka, Z. Hou, O. Yokota, T. Yashima, Study of durable catalyst *Internal Reference*

67 R. Martinez , E. Romero, C. Guimon, R. Bilbao, CO_2 reforming of methane over coprecipitated Ni–Al catalysts modified with lanthanum *Appl. Catal. A: General* **274** (2004), p.139.

Appendix A

This section contains equations employed for calculations and all of the data obtained from the catalyst preparation and equipment calibration.

1 Equations employed for calculations

1-A: Equation for Conversion

$$A = \frac{F_I - F_O}{F_I}$$

A : Conversion of respective reactant
F_I : Inlet flow rate of respective reactant (SCCM)
F_O : Outlet flow rate of respective reactant (SCCM)

1-B: Equation for Selectivity

$$S_{H_2} = \frac{F_{H_2}}{2 \times (F_{CH_{4,I}} - F_{CH_{4,O}})}$$

$$S_{CO} = \frac{F_{CO}}{(F_{CH_{4,I}} - F_{CH_{4,O}}) + (F_{CO_{2,I}} - F_{CO_{2,O}})}$$

$F_{CH_{4,I}}$: Inlet flow rate of CH_4 (SCCM)
$F_{CH_{4,O}}$: Outlet flow rate of CH_4 (SCCM)
F_{CO} : Outlet flow rate of CO (SCCM)
$F_{CO_{2,I}}$: Inlet flow rate of CO_2 (SCCM)
$F_{CO_{2,O}}$: Outlet flow rate of CO_2 (SCCM)
F_{H_2} : Outlet flow rate of H_2 (SCCM)
S_{H_2} : Selectivity of H_2
S_{CO} : Selectivity of CO

1-C: Equation for Reaction Rate

$$R_x = \frac{\Delta F_x}{1000 \times 22.4 \times 60 \times W_{Cat}}$$

ΔF_x : Flow rate of respective reactant consumed during the reaction (SCCM)

R_x : Reaction rate of respective reactant (mol/g-cat/s)

W_{Cat} : Weight of catalyst (g-cat)

2 Introduction to Design Expert 6.0

Design Expert is a Windows-based program, owned by Stat-Ease, which can be used to optimize a process. It provides many powerful statistical tools:

1, Two-level factorial screening studies -- Identify the vital factors that affect the process or product.

2, General factorial studies -- Discover the ideal combination of categorical factors, such as source versus type of raw material supply. Identify the vital factors that affect your process or product.

3, Response surface methods (RSM) -- Find the ideal process settings. Achieve optimal performance.

4, Mixture design techniques -- Discover the optimal formulation.

5, Combinations of process factors, mixture components, categorical factors -- Tailor the design of experiments to what you need to know.

This part of the project was designed using the methodology of RSM with a standard RSM design, Central Composite Design (CCD). CCD's are designed to estimate the coefficient of a quadratic model. A CCD has three groups of design points:

1, Factorial design points—Consists of all possible combinations of the +1 and -1 levels of factors. For this case of two factors there are four design points: (-1,-1), (+1,-1), (-1,+1), and (+1,+1).

2, Axial points—For the two factors design, four axial points are: (-α,0), (α,0), (0,-α), (0,α). The value for α is calculated in each design for both rotatatibility and orthogonality of the blocks. The value of α is 1.41421 in this case.

3, Central points—The middle point of each factor (0,0). Central points are usually repeated 4-6 times to get a good estimate of experimental error. There are five central points generated in this case.

3 Equation Predicted by Design Expert 6.0

$$SA_{BET} = 263.7 + 1.14 * H - 122.7 * AC + 2.97 * H^2 + 1051 * AC^2 - 94.3 * H * AC$$

$$D_{Ave} = 19.3 + 2.71 * H + 5.41 * AC$$

AC : Acid/Alkoxide (0.05-0.35)

D_{Ave} : Average pore diameter (Å)

H : Hydrolysis ratio (1-6)

SA_{BET} : BET surface area (m^2/g)

Table A-1 Recipe of the optimization of the sol-gel process for making 4g 10wt% Ni-Ti catalyst

	Precursor solution					Hydrolysant
Run #	$Ti(BuOH)_4$ (mL)	$Ni(NO_3)_2.6H_2O$ (g)	MeOH (mL)	H_2O (mL)	HNO_3 (mL)	MeOH (mL)
Run 1	1.98	15.4	15	4.9	0.25	5
Run 2	1.98	15.4	15	0.93	0.56	5
Run 3	1.98	15.4	15	3.26	0.56	5
Run 4	1.98	15.4	15	3.26	0.14	5
Run 5	1.98	15.4	15	3.26	0.56	5
Run 6	1.98	15.4	15	5.58	0.56	5
Run 7	1.98	15.4	15	1.61	0.87	5
Run 8	1.98	15.4	15	3.26	0.56	5
Run 9	1.98	15.4	15	3.26	0.98	5
Run 10	1.98	15.4	15	4.9	0.87	5
Run 11	1.98	15.4	15	1.61	0.25	5
Run 12	1.98	15.4	15	3.26	0.56	5
Run13	1.98	15.4	15	3.26	0.56	5

Table A-2 Recipe of the sol-gel process for making 10g of Ni-Ti catalyst under the optimal operation condition

		1wt%	3wt%	5wt%	10wt%
Precursors solution	$Ti(BuOH)_4$ (mL)	42.3	41.4	40.6	38.4
	$Ni(NO_3)_2.6H_2O$ (g)	0.5	1.5	2.5	5
	MeOH (mL)	41.8	40.9	40.1	38
Hydrolysant	H_2O (mL)	11.6	11.4	11.2	10.6
	HNO_3 (mL)	0.55	0.54	0.53	0.50
	MeOH (mL)	20	20	20	20

Table A-3 Recipe of the 10g 5wt% NixTiyAlz catalyst

Precursor Solution				Hydrolysant		
$Ti(BuOH)_4$ (mL)	$Ni(AC)_2.4H_2O$ (g)	$Al_2(NO_3)_3.9H_2O$ (g)	MeOH (mL)	H_2O (mL)	HNO_3 (mL)	MeOH (mL)
20.28	2.12	17.47	40	5.29	0.25	15

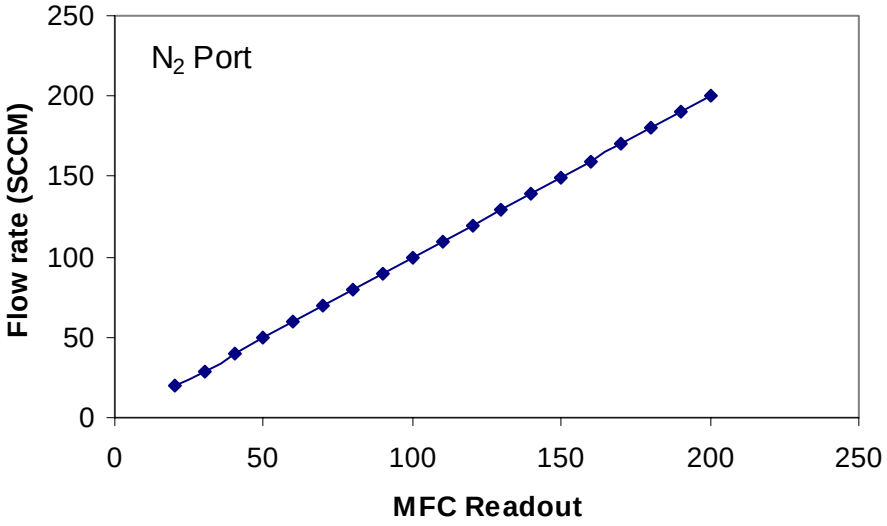

Figure A-1. MFC calibration — N_2 port

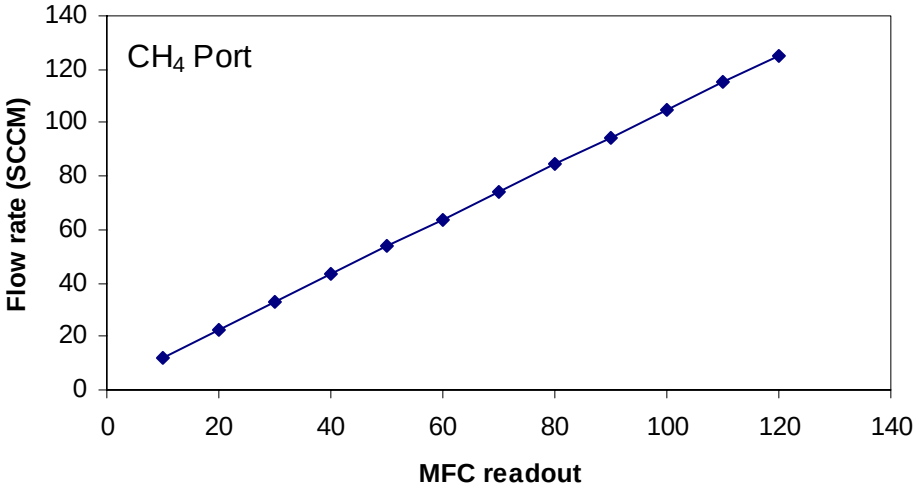

Figure A-2. MFC calibration — CH_4 port

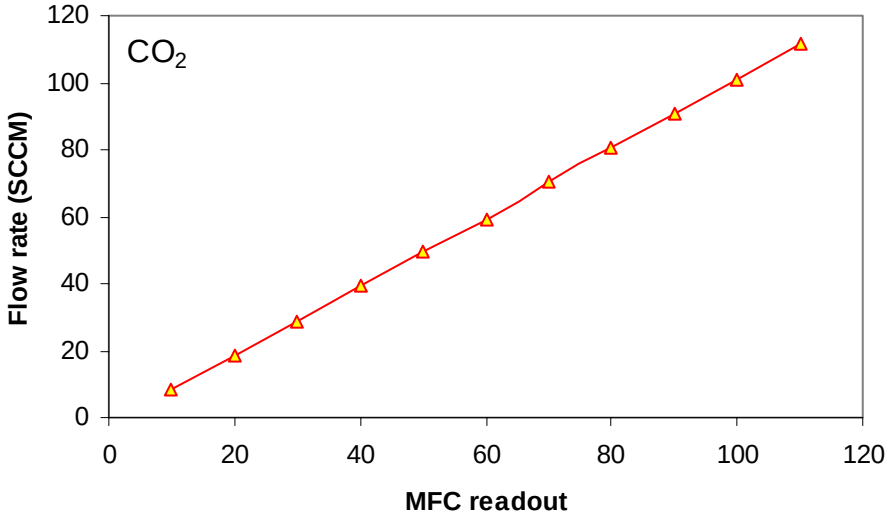

Figure A-3. MFC calibration — CO_2 port

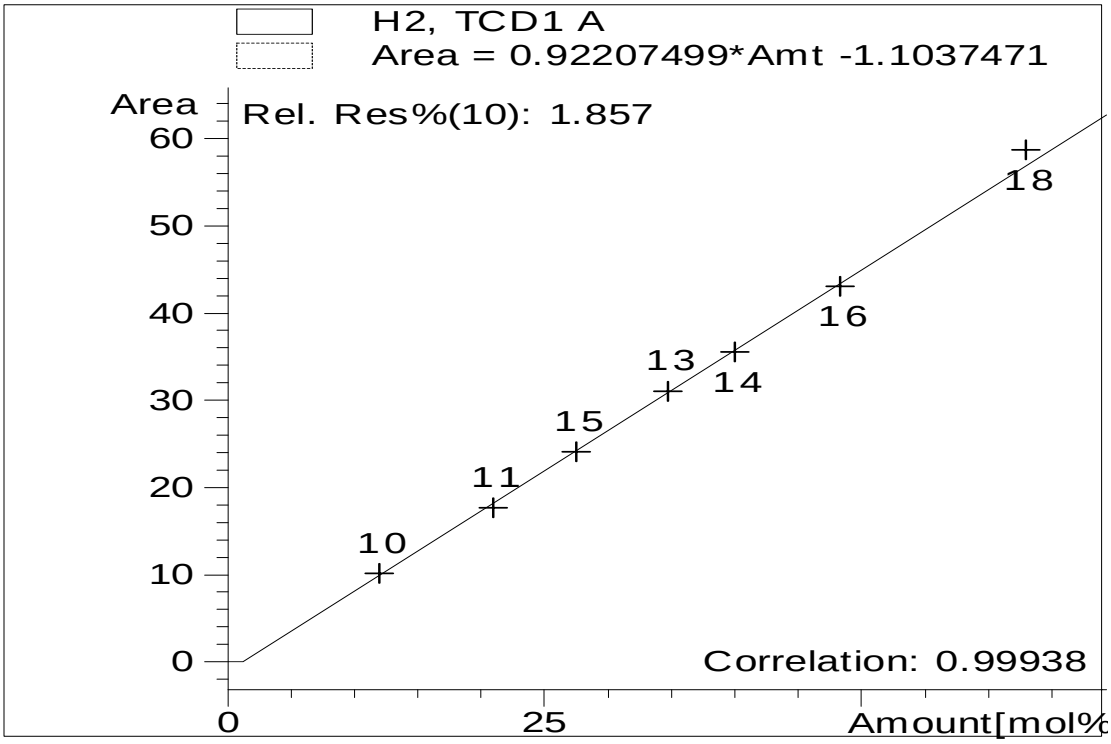

Figure A-4. GC calibration – H_2

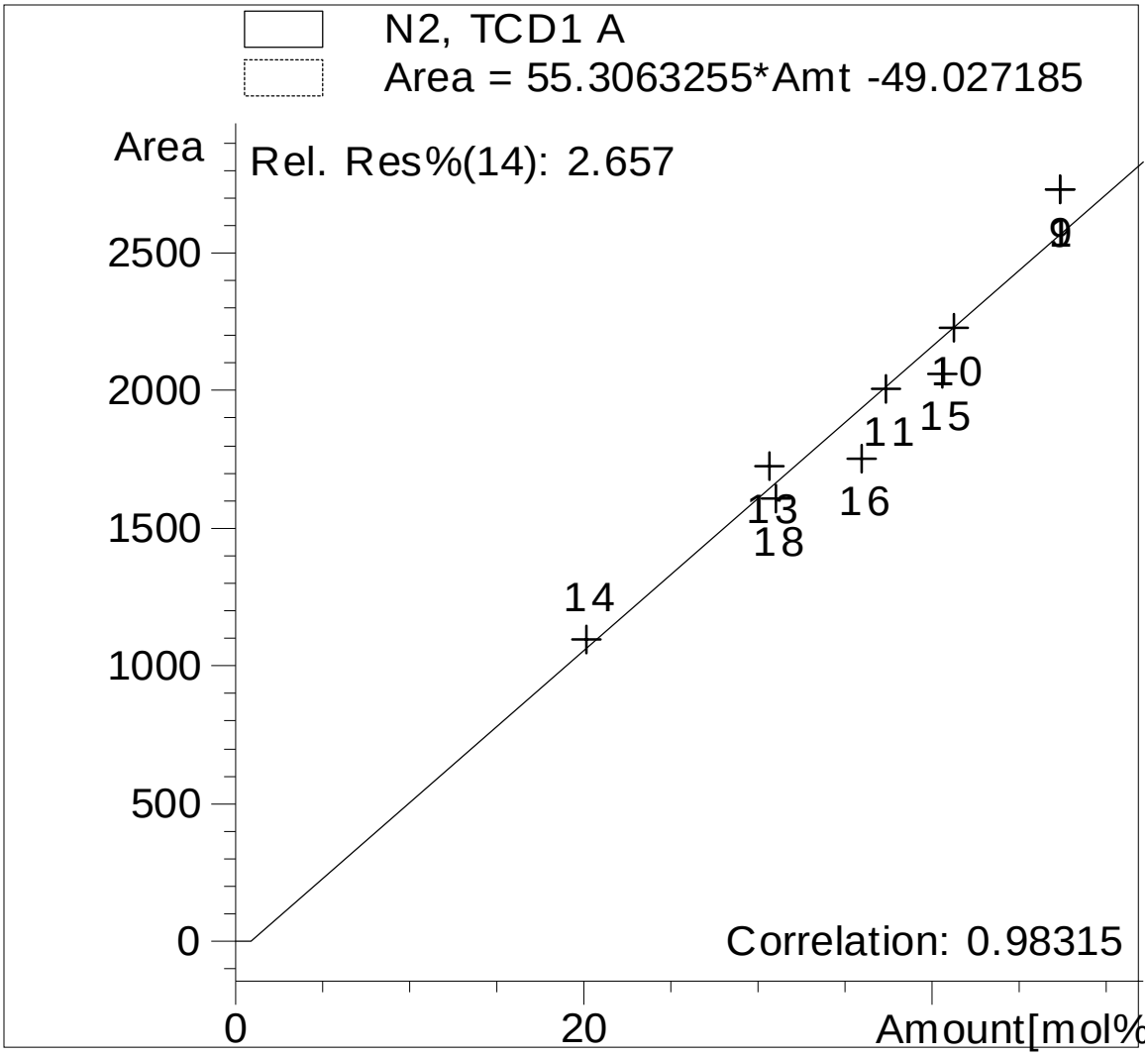

Figure A-5. GC calibration – N_2

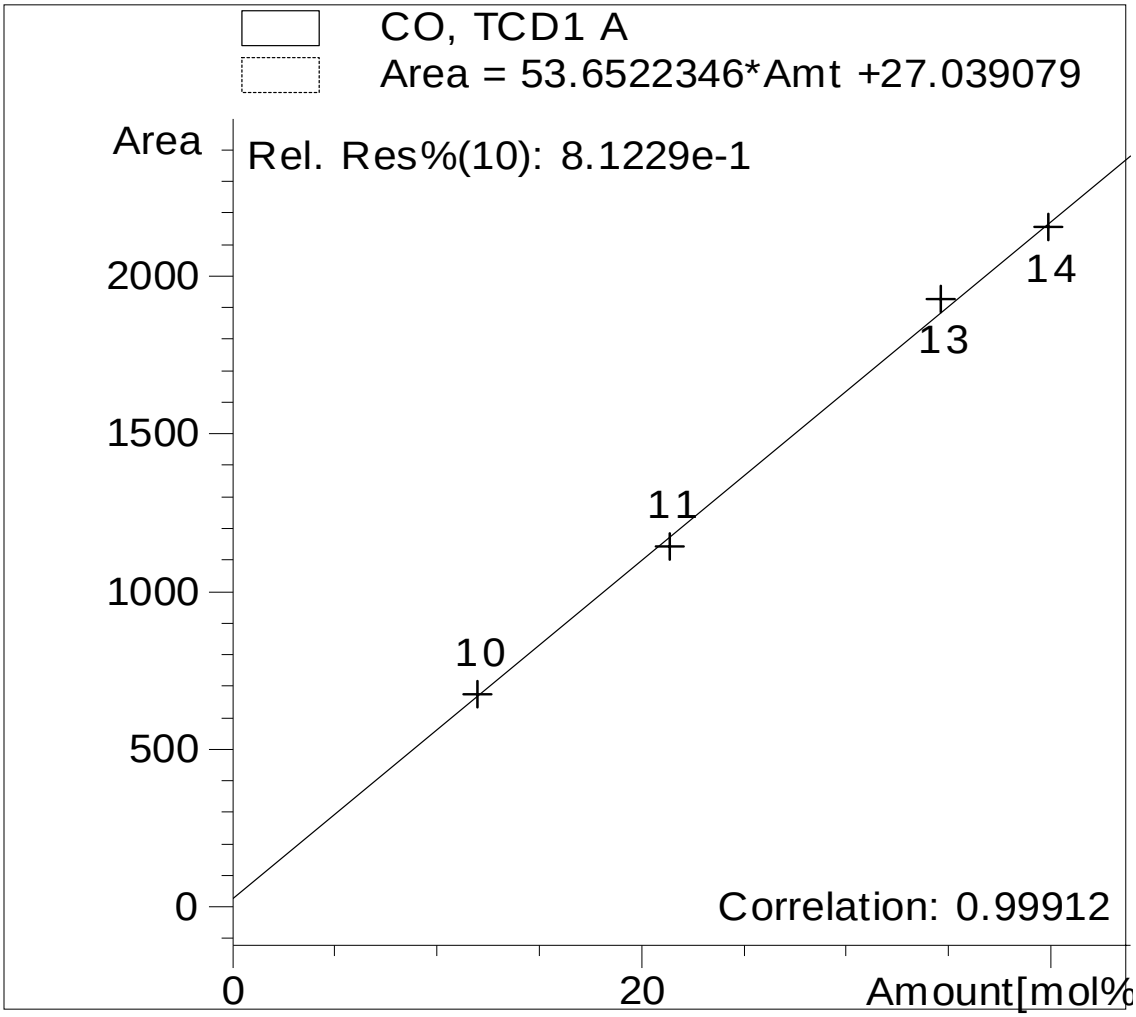

Figure A-6. GC calibration – CO

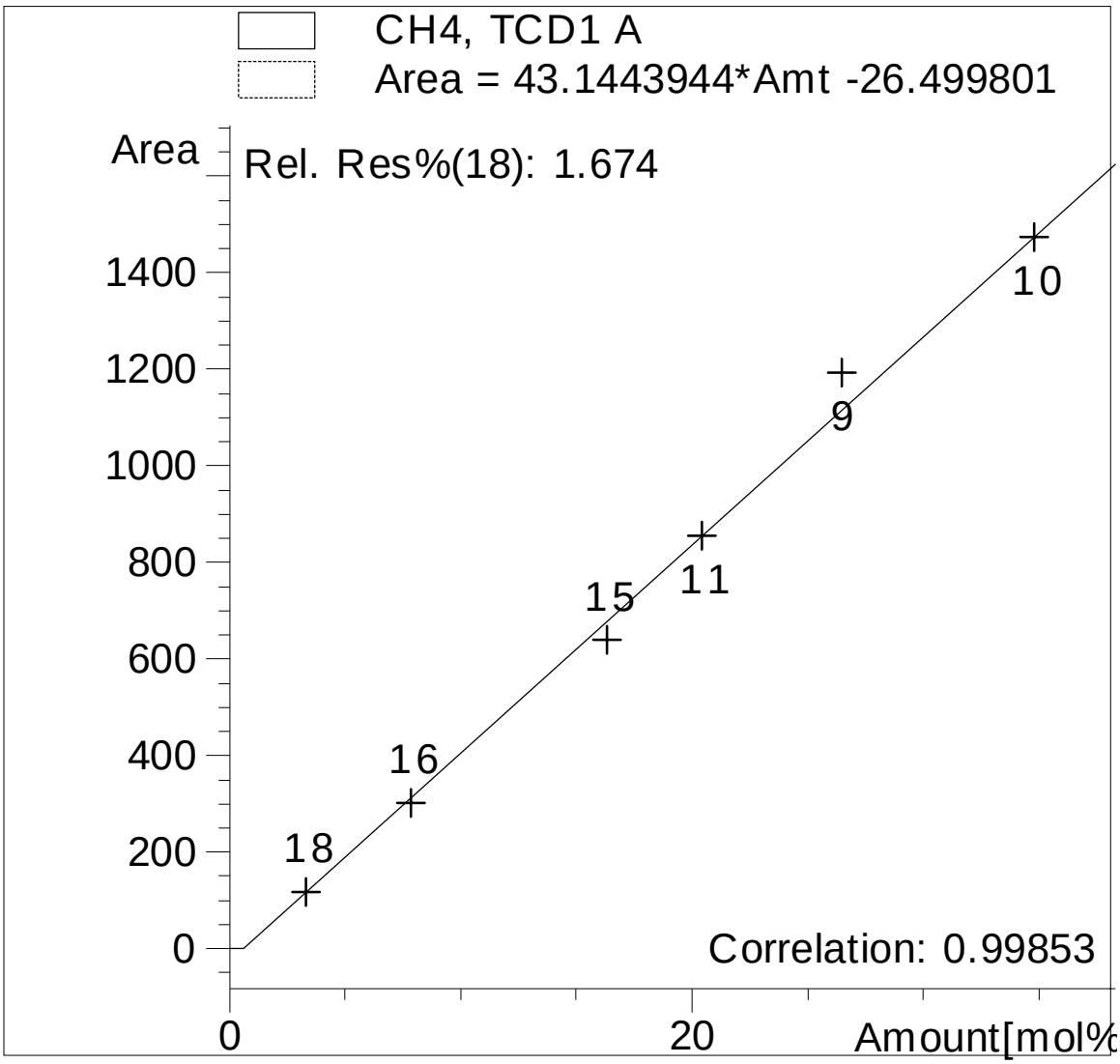

Figure A-7. GC calibration – CH_4

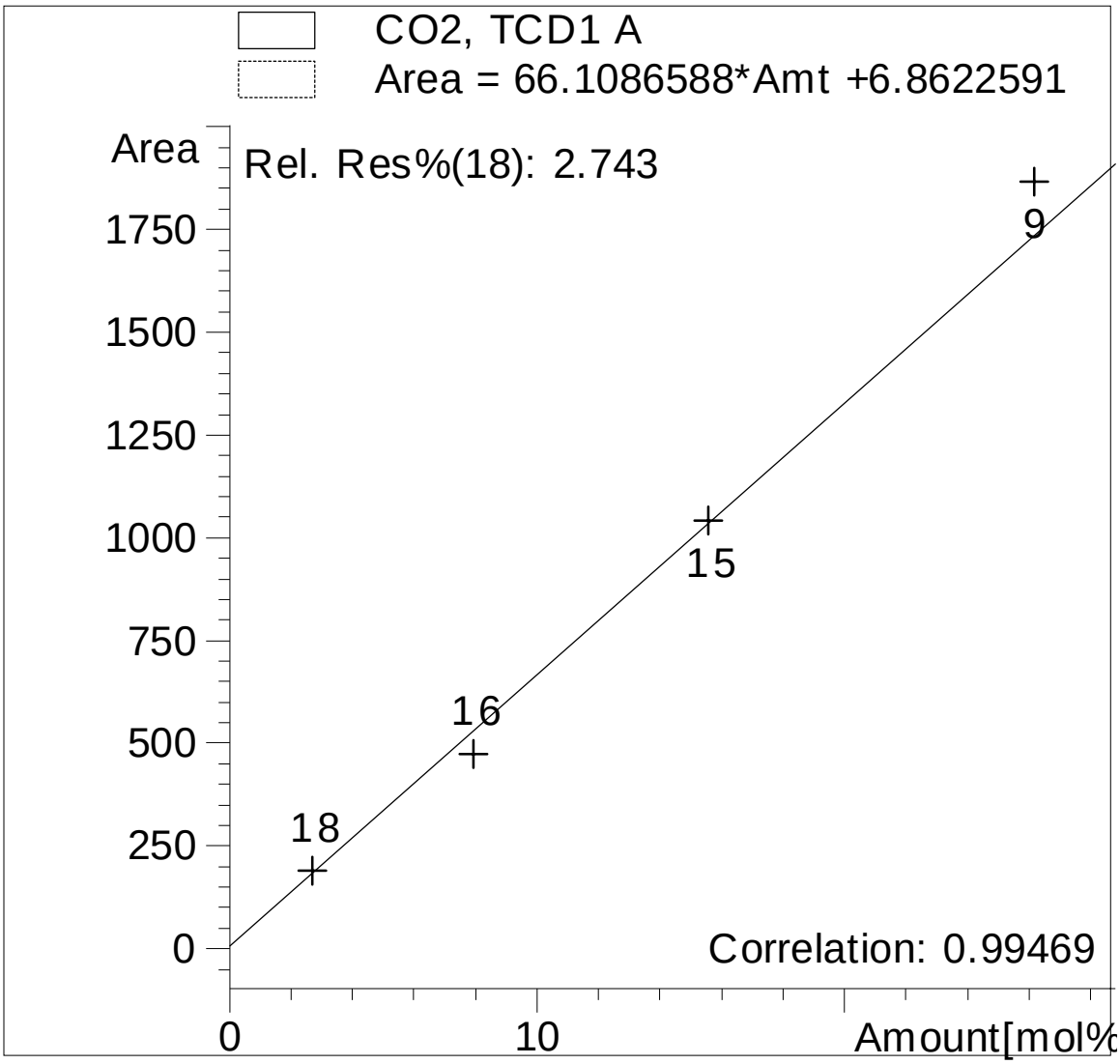

Figure A-8. GC calibration – CO_2

Appendix B

This section contains all of the raw data calculated by GC from the catalyst evaluations

Table B-1 Concentration of gases in effluent for the evaluation of reduction temperature

Temp (K)	H_2(%)	N_2(%)	CO(%)	CH_4(%)	CO_2(%)
823	9.42	41.72	13.47	17.5	17.89
893	22.71	35.5	28.24	7.21	6.33
97	24.74	34.8	30.07	5.56	4.48
1003	17.1	38.21	23.09	11.57	10.07
1023	1.71	45.91	0.33	25.32	26.72
1073	1.65	45.88	0.31	26.09	26.06

Table B-2 Concentration of gases in effluent for the evaluation of reduction time

Time (h)	H_2(%)	N_2(%)	CO(%)	CH_4(%)	CO_2(%)
2	26.59	33.81	31.04	4.55	4.01
4	24.74	34.8	30.07	5.56	4.84
6	21.78	36.1	27.82	7.63	6.68

Table B-3 Concentration of gases in effluent for the evaluation of feed rate

Linear velocity (m/s)	H_2(%)	N_2(%)	CO(%)	CH_4(%)	CO_2(%)
0.05	25.62	34.41	31.18	4.67	4.1
0.15	18.05	38.78	23.64	11.19	8.34
0.25	13.87	41.32	19	14.51	11.3
0.35	11.02	42.39	16.2	16.91	13.47

Table B-4 Concentration of gases in effluent for the evaluation of 1wt% Ni-Ti catalyst

Time (h)	H_2(%)	N_2(%)	CO(%)	CH_4(%)	CO_2(%)
0	2.39	46.75	0.69	25.46	24.72
1	1.51	47.88	0.01	25.64	24.96
2	1.7	47.19	0	25.89	25.21
3	0	48.07	0	26.31	25.61
4	0	47.97	0	26.34	25.69

Table B-5 Concentration of gases in effluent for the evaluation of 3wt% Ni-Ti catalyst

Time (h)	H_2(%)	N_2(%)	CO(%)	CH_4(%)	CO_2(%)
0	10.68	42.81	16.85	16.5	13.17
1	8.71	43.9	14.39	18.12	14.89
2	7.39	44.02	12.61	19.53	16.44
3	6.39	44.89	10.89	20.31	17.51
4	5.6	44.91	9.6	21.26	18.62

Table B-6 Concentration of gases in effluent for the evaluation of 5wt% Ni-Ti catalyst

Time (h)	H_2(%)	N_2(%)	CO(%)	CH_4(%)	CO_2(%)
0	12.28	41.67	18.32	15.53	12.21
1	10.02	43.05	15.74	17.24	13.94
2	8.98	43.37	14.65	18.32	14.68
3	8.17	43.82	13.5	18.87	15.65
4	7.3	44.24	12.55	19.53	16.37

Table B-7 Concentration of gases in effluent for the evaluation of 10wt% Ni-Ti catalyst

Time (h)	H_2(%)	N_2(%)	CO(%)	CH_4(%)	CO_2(%)
0	20.35	37.88	25.24	9.63	6.9
1	17.16	39.57	22.55	11.78	8.94
2	15.68	39.97	21.2	13	10.15
3	14.9	40.38	20.17	13.74	10.8
4	13.96	41.23	19.17	14.26	11.37

Table B-8 Concentration of gases in effluent for the evaluation of 5wt% Ni-Ti-Al catalyst

Time (h)	H_2(%)	N_2(%)	CO(%)	CH_4(%)	CO_2(%)
0	19.11	38.12	22.26	11.2	9.32
1	19.9	37.17	23.19	10.81	8.93
2	20.02	37.24	23.27	10.7	8.77
3	19.86	37.48	23.23	10.7	8.73
4	19.95	37.06	23.46	10.77	8.76
7	19.56	37.54	23.29	10.83	8.78
10	19.5	37.22	23.27	10.49	9.51